Improving the representation of HONO chemistry in CMAQ and examining its impact on haze over China

Shuping Zhang,[1,2,3] Golam Sarwar,[4] Jia Xing,[2] Biwu Chu,[1,3,5] Chaoyang Xue,[1,3] Arunachalam Sarav,[6] Dian Ding,[2] Haotian Zheng,[2] Yujing Mu,[1,3,5] Fengkui Duan,[2] Tao Ma,[2] Hong He[1,3,5]

[1]State Key Joint Laboratory of Environment Simulation and Pollution Control, Research Center for Eco-Environmental Sciences, Chinese Academy of Sciences, Beijing 100085, China

[2]State Key Joint Laboratory of Environment Simulation and Pollution Control, School of Environment, Tsinghua University, Beijing 100084, China

[3]University of Chinese Academy of Sciences, Beijing 100049, China

[4]Center for Environmental Measurement and Modeling, U.S. Environmental Protection Agency, 109 T.W. Alexander Drive, Research Triangle Park, NC, 27711, USA

[5]Center for Excellence in Regional Atmospheric Environment, Institute of Urban Environment, Chinese Academy of Sciences, Xiamen 361021, China

[6]Institute for the Environment, The University of North Carolina at Chapel Hill, 100 Eurpoa Drive, Chapel Hill, NC 27514, USA

Correspondence to: Golam Sarwar(Sarwar.Golam@epa.gov), Jia Xing(xingjia@tsinghua.edu.cn), Hong He(honghe@rcees.ac.cn)

Abstract. We compare Community Multiscale Air Quality (CMAQ) model predictions with measured nitrous acid (HONO) concentrations in Beijing, China for December 2015. The model with the existing HONO chemistry in CMAQ severely under-estimates the observed HONO concentrations with a normalized mean bias of -97%. We revise the HONO chemistry in the model by implementing six additional heterogeneous reactions in the model: reaction of nitrogen dioxide (NO_2) on ground surfaces, reaction of NO_2 on aerosol surfaces, reaction of NO_2 on soot surfaces, photolysis of aerosol nitrate, nitric acid displacement reaction, and hydrochloric acid displacement reaction. The model with the revised chemistry substantially increases HONO predictions and improves the comparison with observed data with a normalized mean bias of -5%. The photolysis of HONO enhances day-time hydroxyl radical by almost a factor of two. The enhanced hydroxyl radical concentrations compare favourably with observed data and produce additional sulfate via the reaction with sulfur dioxide, aerosol nitrate via the reaction with nitrogen dioxide, and secondary organic aerosols via the reactions with volatile organic compounds. The additional sulfate stemming from revised HONO chemistry improves the comparison with observed concentration; however, it does not close the gap between model prediction and the observation during polluted days.

1 Introduction

China has been suffering from haze pollution (Lelieveld et al., 2015) in which secondary particles contribute more than 70% to the haze formation (Guo et al., 2014; Huang et al., 2014; Quan et al., 2014; Zheng et al., 2015). However, the mechanism for the formation of high levels of secondary particles is

not yet clearly understood and most current air quality models tend to under-estimate particle concentrations compared with observed data in China. Several secondary particle formation pathways have been proposed, such as ①sulfate (SO_4^{2-}) formation via the heterogeneous oxidation of sulfur dioxide (SO_2) promoted by hydrogen peroxide (H_2O_2) and/or ②nitrogen dioxide (NO_2) on mineral dust (He et al., 2014; Huang et al., 2015; Ye et al., 2018), ③aqueous-phase oxidation of SO_2 promoted by NO_2 in particle-bound water film (Wang et al., 2016; Li et al., 2017), ④aqueous-phase oxidation of SO_2 by nitrous acid (HONO) produced from the photolysis of aerosol nitrate (NO_3^-) in particle-bound water (Wang et al., 2016; Li et al., 2017), and ⑤NO_3^- formation via efficient hydrolysis of dinitrogen pentoxide (N_2O_5) on aerosol surfaces (Wang et al., 2017; Kulmala, 2018). However, the gap between the model predictions and observed SO_4^{2-} is persistent and still large (Zhang et al., 2019c).

Previous studies suggested that the underestimation of atmospheric oxidation capacity during haze limited the formation of secondary particles (Sun et al., 2013; Gen et al., 2019; Tsona and Du, 2019). As a hydroxyl radical (OH) source, HONO plays an important role in the oxidation of precursors (Stutz et al., 2002; Kleffmann et al., 2005). However, the large underestimation of HONO (up to the ppb level) is prevalent during haze simulations around the world (Li et al., 2012; Fu et al., 2019; Zhang et al., 2019d). Moreover, HONO underestimation is reported to be highly related to the formation of fine particulate matter ($PM_{2.5}$) (Wang et al., 2015; Xue et al., 2020), particularly for secondary $PM_{2.5}$. Compared with summer, HONO concentrations in winter tend to be high when secondary particle underestimation occurs (Li et al., 2018a; Zhang et al., 2019b). The underestimation of HONO may partly explain the phenomenon of insufficient oxidant for the formation of secondary particles during the winter haze (Li et al., 2018b; Li et al., 2018c).

Sarwar et al. (2008) compared the CMAQ predictions with HONO concentrations measured in Philadelphia, PA, USA, during a summer month (July 2001) and reported that the model with only gas-phase chemistry seriously under-estimates observed concentrations. They implemented HONO emissions from motor vehicles, the heterogeneous reaction on the ground and aerosol surfaces, and the photolysis of nitric acid (HNO_3) deposited on environmental surfaces, which improved predicted HONO concentrations; however, the underprediction persisted. The model with the revised chemistry enhanced OH and ozone (O_3) concentrations. Li et al. (2010) examined the impact of HONO chemistry in Mexico City using the Weather Research and Forecasting model, coupled with chemistry (WRF-CHEM). They considered five different HONO reactions: ① the existing homogeneous reaction between NO (nitric oxide) and OH, ② the added heterogeneous reaction of NO_2 on the aerosol surfaces, ③ the added heterogeneous reaction of NO_2 on the ground surfaces, ④the added heterogeneous reaction of NO_2 with semi-volatile organics, and ⑤ the added heterogeneous reaction of NO_2 reaction with freshly emitted soot. The model successfully reproduced observed HONO concentrations in Mexico City during March 2006. The model with the HONO chemistry increased OH, HO_2 (hydroperoxyl radical), O_3, secondary organic aerosols (SOA), NO_3^-, and ammonium (NH_4^+) and improved the comparison with observed data. The enhancements were particularly high in the morning. However, the impact on SO_4^{2-} was negligible. Czader et al. (2012) compared CMAQv5.3 predictions with HONO measured during August and September 2006 in Houston, TX, USA, and also reported that the model with gas-phase alone was not sufficient to explain the observed data and predicted concentrations. They added HONO emissions, NO_2 hydrolysis, active NO_2 chemistry, and conversion of NO_2 into HONO on organic materials covered surfaces, which improved model performance for

HONO and, subsequently, increased OH and O_3 concentrations.

Fu et al. (2019) studied a 5-day episode (January 4-8, 2017) in the Pearl River Delta of China during which high levels of particles, O_3, and HONO concentrations were measured. They implemented four additional reactions for HONO production into the model: ① relative humidity-dependent heterogeneous reaction of NO_2, ②light-dependent heterogeneous reaction of NO_2, ③photolysis of NO_3^-, and ④photolysis of HNO_3 on surfaces. The model with the additional chemistry successfully reproduced measured HONO concentrations which subsequently enhanced and improved O_3 and $PM_{2.5}$ predictions. Xing et al. (2019) examined the impact of HONO chemistry on SOA in the Beijing-Tianjin–Hebei area (BTH) of China using the WRF-CHEM model during January 9-26, 2014. They employed the homogeneous and heterogeneous HONO chemistry of Li et al. (2010) and reported that the HONO chemistry could increase the average SOA concentration by ~46%. Zhang et al. (2019a) employed the WRF-CHEM model to examine the impact of HONO chemistry on OH, HO_2, and SOA concentrations in the BTH region during a winter haze period (November 29–Dec. 3, 2017). They employed six HONO sources in the model: ① traffic emissions, ② soil emissions, ③ biomass burning emissions, ④indoor emissions, ⑤heterogeneous reaction on aerosol surfaces, and ⑥ heterogeneous reaction on ground surfaces. The model reproduced observed HONO concentrations and substantially elevated OH, HO_2, and SOA concentrations.

In this study, we employ the Community Multiscale Air Quality (CMAQ) model to simulate and compare HONO predictions with observed data from the field campaign in Beijing. The field campaign was conducted during December 7-22, 2015, in Beijing, China, during which high concentrations of HONO and aerosols were measured.

2 Methodology

2.1 Modeling framework and homogeneous HONO chemistry

The Community Multiscale Air Quality (CMAQv5.3) (USEPA, 2019) (https://www.epa.gov/cmaq) was used widely in this study. CMAQv5.3 includes the representation of important atmospheric processes and has been used widely in air quality studies in many countries, including China (Byun and Schere, 2006; Sarwar et al., 2008; Xing et al., 2015). The modeling domain, which covered China and consisted of 182 × 232 horizontal grid-cells with a 27 × 27 km horizontal resolution and 14 vertical layers encompassing surface to 100 hPa. The first layer height of the model was about 36 m. The static initial and boundary conditions from CMAQv5.3 were used for the study. A 22-day model spin-up period was used to minimize the effect of initial conditions on model predictions. The Carbon Bond 6 (version 3, CB6r3) (Emery et al., 2015) chemical mechanism that contain six homogeneous reactions related to HONO (**错误!未找到引用源。**) was used without any modification. The calculated equilibrium constant in CB6 (Kaiser and Wu, 1977) is similar to reported rate constants by Chan et al (5×10^{-20} in CB6 vs. 6×10^{-20} in Chan et al. (Chan et al., 1976a; Chan et al., 1976b).CMAQv5.3 contains a treatment of heterogeneous conversion of NO_2 at aerosol and ground surfaces (Sarwar et al., 2008), in which uptake coefficient at aerosol surfaces and aera density of ground surfaces were revised in this study (Section 2.2). CMAQv5.3 accounts for HONO emissions from motor vehicles as 0.008 × NO_x emissions which were kept the same (NO_X = oxides of nitrogen, NO+NO_2). Photolysis rate

coefficients (min^{-1}) in CMAQv5.3 (J-values) are computed for photo dissociation reactions by Eq. (1). Absorption cross-section and quantum yield data suggested by the International Union of Pure and Applied Chemistry (IUPAC) are used for calculating photolysis rate coefficients of HONO (Table 1) (http://iupac.pole-ether.fr/htdocs/datasheets/pdf). Absorption cross-section and quantum yield data suggested by the IUPAC for NTR (organic nitrate) are used for calculating photolysis rate coefficients of CRON (nitro-cresol) (Table 1) (http://iupac.pole-ether.fr/htdocs/datasheets/pdf).

$$J_i = \int_{\lambda 1}^{\lambda 2} F(\lambda)\sigma_i(\lambda)\phi_i(\lambda)d\lambda \quad (1)$$

Note: $F(\lambda)$ is the actinic flux (photons cm^{-2} min^{-1} nm^{-1}), $\sigma_i(\lambda)$ the absorption cross section for the molecule undergoing photo dissociation (cm^2 $molecule^{-1}$), $\Phi_i(\lambda)$ the quantum yield of the photolysis reaction (molecules $photon^{-1}$), and λ the wavelength (nm).

We also instrumented the model with the Integrated Reaction Rate (IRR) option, which enabled estimating the contribution of each reaction to the predicted HONO concentrations (Czader et al., 2013). The Sulfur Tracking Model in CMAQv5.3 was used to quantitatively calculate the contribution of each reaction to predicted SO_4^{2-} concentration (Mathur et al., 2008).

Table 1: Gas-phase chemical reactions related to HONO in CB6r3

Reaction Number	Reaction	Reaction Rate Constant (k)
1	NO + OH = HONO	$k = \left\{\frac{k_0[M]}{(1+k_0[M]/k_1)}\right\} 0.81^{\left\{1+\left[log_{10}\left(\frac{k_0[M]}{k_1}\right)/0.87\right]^2\right\}^{-1}}$ $k_0 = 7.4\times10^{-31}\left(\frac{T}{300}\right)^{-2.4}$ $k_1 = 3.3\times10^{-11}\left(\frac{T}{300}\right)^{-0.3}$
2	$NO + NO_2 + H_2O$ = 2.0×HONO	$k = 5.0\times10^{-40}$
3	HONO + HONO = $NO + NO_2 + H_2O$	$k = 1.0\times10^{-20}$
4	HONO = NO + OH	J_{HONO}
5	HONO + OH = NO_2	$k = 2.5\times10^{-12}e^{(260/T)}$
6	CRON = HONO + HO_2 + FORM + OPEN	J_{NTR}

Note: NO = nitric oxide, NO_2 = nitrogen dioxide, OH = hydroxyl radical, HO_2 = hydroperoxy radical, H_2O = water vapor, HONO = nitrous acid, CRON = nitro cresol; FORM = formaldehyde, OPEN = aromatic ring open product, [M] = total pressure ($molecules/cm^3$), T = air temperature (K), and k = rate constant. First-order rate constants are in units of s^{-1}, second-order rate constants are in units of cm^3

molecule^{-1} s^{-1}, third-order constants are in units of cm^{6} molecule^{-2} s^{-1}. CMAQv5.3 converts cm-molecule-s units into ppm-min units before solving the system of ordinary differential equations for chemistry. J_{HONO} = photolysis of HONO, and J_{NTR} = photolysis of NTR (organic nitrate)..

2.2 Heterogeneous HONO chemistry

The heterogeneous formation of HONO has been studied for several decades (Fig.S1). The long research history of HONO heterogeneous reaction can be found in Finlayson-Pitts (2000). The understanding of heterogeneous HONO chemical reactions and parameter method is evolving. Investigators have proposed hydrolysis of NO_2 on the humid aerosol surfaces, heterogeneous conversion of NO_2 on ground surfaces, photolysis of NO_3^-, catalytical formation on soot particles and acid displacement process in the atmosphere during the past several years (Stemmler et al., 2006; Liu et al., 2014; Karamchandani et al., 2015; VandenBoer et al., 2015; Tong et al., 2016; Ye et al., 2016; Ye et al., 2017; Lu et al., 2018; Gen et al., 2019; Xu et al., 2019; Zhang et al., 2019d). Xue et al. (2020) and Liu et al. (2019) recently measured summertime atmospheric HONO concentrations in a rural area in China and performed simulations using a box model with updated chemical reactions for HONO production published in the literature. They reported that the simulations generally reproduced observed HONO concentrations using the updated HONO chemical reactions. However, the box model did not consider horizontal and vertical transportation, limiting the impact of HONO formation on air quality. We implement these updated chemical reactions into a three-dimensional (3D) air quality model, CMAQv5.3, to examine their impacts on air quality.

Hydrolysis processes on the humid aerosol surfaces is an important HONO-producing reaction in the atmosphere (An et al., 2012; Cui et al., 2018). And we use the uptake coefficient (Table 2) employed by Liu et al. (2019) at night-time (Reaction 7a). The selection criteria and possible ranges of the uptake coefficient are discussed in SI. The reaction on aerosols can be enhanced by light (Zhang et al., 2019b); thus, we use a radiation-dependent uptake coefficient during day-time (Reaction 7b). We use CMAQv5.3-calculated aerosol surface area-to-volume ratio (S/V_a) to calculate rate constant for the reaction on aerosol surfaces. Heterogeneous conversion of NO_2 on ground surfaces also has been studied intensively in the laboratory and field (Li et al., 2018a). Vertical night-time profile measurements suggest that heterogeneous HONO formation on the ground is the dominant reaction; thus, we also use this reaction. Similar to the heterogeneous reaction on aerosol surfaces, we employ an uptake coefficient used by Liu et al. (2019) for the reaction at night (Reaction 8a) and a radiation-dependent uptake coefficient during day-time (Reaction 8b). Following the suggestions of Vogel et al. (2003), Li et al., (2019) and Liu et al., (2019), we use a value of 1.7/H (S/Vg =1.7S'/HS'= 1.7/H, S' represents the geometric surface area of the first layer. 1.7 is the effective surface factor per ground surface in first layer. H is the model's first-layer height.) for surface area-to-volume ratio of ground (S/Vg) to calculate the rate constant for the reaction on ground surfaces. We also conducted sensitivity analysis by using the value of 2.2/H which is suggested from Voogt and Oke(1997). The result suggests slightly higher concentrations but with similar model performance (details in Figure S4 in Supplemental Information).

Ye et al. (2016) proposed that the photolysis of NO_3^- can lead to HONO production in the atmosphere and reported that its photolysis rate coefficients can be several hundred times faster than the photolysis

rate coefficients of HNO_3. Bao et al. (2018) also reported similar photolysis rate coefficients of NO_3^-. Fu et al. (2019) used this high photolysis rate coefficient in their study to examine the winter-time HONO production in Hong Kong. However, Romer et al. (2018) reported that such high photolysis rate coefficients of NO_3^- are not consistent with observed data over the Yellow Sea and should not be used in air quality models. They suggested that the photolysis rate coefficients of NO_3^- in air quality models should be 1 to 30 times the photolysis rate coefficient of HNO_3. For photolysis of NO_3^-, we use a photolysis rate coefficient of 30 times the photolysis rate coefficient of HNO_3 (Reaction 9).

HONO formation on soot particles can be catalytically enhanced in the presence of artificial solar radiation and lead to persistent reactivity of soot over long periods (Monge et al., 2010). The surface of soot particles as a heterogeneous conversion media has been reported by several studies (Monge et al., 2010; Liu et al., 2014; Spataro and Ianniello, 2014; Cui et al., 2018). The reported heterogeneous uptake coefficient on soot ranges from 10^{-8} to 10^{-6}, with HONO yields ranging between 50% and 100% (Spataro et al., 2013). This heterogeneous soot photochemistry potentially may contribute to day-time HONO concentration. We also employ the reaction using the upper limit of the reported uptake coefficient and calculate the HONO formation rate following Spataro et al. (2013) (Reaction 10).

VandenBoer et al. (2013) reported that deposited HONO can react with carbonates or soil at night and, subsequently, be released from the soil during the day by reactions with atmospheric HNO_3 and HCl (hydrochloric acid). They suggest that this acid displacement process can contribute to a substantial fraction of day-time HONO. We also use this process (Reactions 11 and 12) and employ a parameter similar to that of Liu et al. (2019), except that we utilize a displacement efficiency of 6% for HNO_3 and 20% for HCl following VandenBoer et al. (2015). The dry deposition velocities of HNO_3 and HCl in CMAQ is calculated using a big-leaf resistance model (Wesely, 1989; Wesely, 2007). Calculated deposition velocities fall in the reported ranges of values by Jaeglé et al. (2018) (details in Supplemental Information).

Zhou et al., (2003) reported that HNO_3 deposited on environmental surfaces can undergo rapid photolysis leading to day-time HONO production. Several studies (Sarwar et al., 2008; Fu et al., 2019; Liu et al., 2019) included such a reaction in their models. However, we do not include it because the rate constant has high uncertainty and it could also pose a problem for performing long-term model simulations. For long-term (annual and multiyear) that the deposited amount of HNO_3 could accumulate with time, which could continue increasing the HONO production rates with time. Soil can emit HONO and other nitrogen-containing compounds (Su et al., 2011; Oswald et al., 2013). Rasool et al. (2019) implemented these emissions into CMAQv5.3 by using a mechanistic representation of the underlying processes and examined their impacts on air quality over North America. The impacts of HONO emitted from soil are generally low, and we do not include these emissions in this study.

Table 2 Heterogeneous HONO reactions used in this study

Reaction No.	**Reaction**	**Reaction Rate Constant (k)**	**Uptake coefficient (γ)**	**Reference**
7a.	NO_2 + aerosol = 0.5×HONO + 0.5×HNO_3	$k = \frac{1}{4}\gamma v_{NO2}\frac{S}{V_a}$	$\gamma_{an} = 8\times10^{-6}$	(Liu et al., 2019)

7b.	NO_2 + aerosol + hv = 0.5×HONO + 0.5×HNO_3	$k = \frac{1}{4}\gamma v_{NO2}\frac{S}{V_a} \times \frac{J}{J_{max}}$	γ_{ad} = 1×10^{-3}	(Liu et al., 2019)
8a.	NO_2 + ground = HONO	$k=\frac{1}{8}\gamma v_{NO2}\frac{1.7}{H}$	γ_{gn} = 4×10^{-6}	(Li et al., 2018a; Liu et al., 2019)
8b.	NO_2 + ground + hv = HONO	$k=\frac{1}{8}\gamma v_{NO2}\frac{1.7}{H} \times \frac{J}{J_{max}}$	γ_{gd} = 6×10^{-5}	(Liu et al., 2019)
9	NO_3^-+ hv = 0.67×HONO + 0.33×NO_2	$J = 30\times J_{HNO3}$		(Romer et al., 2018)
10	NO_2 + EC= 0.61×HONO + 0.39×NO	$k = \frac{1}{4}\gamma v_{NO2}\frac{S\_BET}{V}$	γ = 2×10^{-6}	(Spataro and Ianniello, 2014)
11	HNO_3 + $NaNO_2$ (s) = HONO + $NaNO_3$ (s)	$k=0.06V_{dep\_HNO3}/H$		(VandenBoer et al., 2015)
12	HCl + $NaNO_2$ (s) = HONO + NaCl (s)	$k=0.2V_{dep\_HCl}/H$		(VandenBoer et al., 2015)

Note:

k = first order rate constant (sec^{-1}), γ = heterogeneous uptake coefficient (-), γ_{an} = night-time heterogeneous uptake coefficient on aerosol, γ_{ad} = day-time heterogeneous uptake coefficient on aerosol, γ_{gn} = night-time heterogeneous uptake coefficient on ground, γ_{gd} = day-time heterogeneous uptake coefficient on ground, S/V_a= density of aerosol surface; S/V_g= density of ground surface; v = mean molecular speed (m/s), HNO_3 = nitric acid, $NaNO_2$ = sodium nitrite, NaCl = sodium chloride, J = NO_2 photolysis rate coefficient, J_{max} = maximum NO_2 photolysis rate coefficient, V_{dep_HNO3} = deposition velocity of HNO_3 (m/s), V_{HCl} = deposition velocity of HCl (m/s), H = the first-layer height (m), and S_BET/V = BET surface area-to-volume ratio that we calculate as follows: CMAQv5.3 predicted elemental carbon (EC) (μg/m^3) × 1.0 ×10^{-6} (g/μg) ×122 m^2/g, NO_3^- = aerosol nitrate, EC= elemental carbon. Reactions 7a, 7b, 8a, and 8b are revised from CMAQv5.3, while reaction numbers 9 ,10, 11 and 12 are newly added reactions.

2.3 Simulation cases

We performed two different simulations using CMAQv5.3 for December 7-22, 2015. One simulation denoted by "ORI" used the gas-phase HONO chemistry in CB6r3 along with the heterogeneous hydrolysis of NO_2 in CMAQv5.3. The implementation of the heterogeneous hydrolysis of NO_2 in CMAQ has previously been described by Sarwar et al. (2008). They accounted for aerosol surface area as well as the ground surface area provided by leaves and building and other structures. Leaf area was estimated using 2 × LAI/H (LAI is the leaf area index and H is the surface layer height in the model) while building and other structure surface areas were estimated using 0.002 × PURB (PURB = percent urban area of a grid-cell in the model). The other simulation denoted by "REV" used the gas-phase HONO chemistry in CB6r3 and the heterogeneous reactions presented in Table 2. For this simulation, we removed the heterogeneous hydrolysis of NO_2 in CMAQv5.3 and used the heterogeneous reactions presented in Table 2. Both simulations used the same HONO emissions (section 2.1). We also completed several additional sensitivity simulations as discussed in Section 3.0.

We used the ABaCAS national emissions inventory (http://www.abacas-dss.com) which resulted in great performance in simulating both NO_2 and fine particle ($PM_{2.5}$). In previous studies, Zhao et al.

(2018) and Zheng et al. (2019) used these emissions and reported a normalized mean bias of 4% for NO_2 and -17% for $PM_{2.5}$ (Normalized Mean Bias (NMB)=$100\times\sum(M_i-O_i)/\sum O_i$, O_i is observed HONO concentration, and M_i is the simulated HONO concentration in model (Jaeglé et al., 2018)). Meteorological fields for CMAQv5.3 were simulated using the Weather Research and Forecasting model version 3.8 (WRFv3.8) (Skamarock and Klemp, 2008). WRF has consistent parameterization for cloud fraction simulation, as well as other climate models (see (Xu and Krueger, 1991) and (Xu and Randall, 1996) for a review on this topics). We compared WRF predictions with observed temperature, wind speed, and water vapor mixing ratio in China (Fig. S2). Mean bias (MB) and root mean square error (RMSE) for temperature, wind speed and MB for water vapor mixing ratio meet the benchmark limits suggested by Emery et al.(2001).

2.4 Observation data

A field campaign was conducted during December 7-22, 2015, at the Research Center for Eco-Environmental Sciences (40.01° N, 116.35° E) to measure atmospheric pollutants and meteorological parameters. Atmospheric concentrations of HONO were measured using a stripping coil (SC) equipped with ion chromatograph (IC). The details of the instrument have been described elsewhere (Xue et al., 2019a). We also completed a statistical analysis of the measurements from the instrument with data from three other methods and concluded that it can provide reliable measurements. The instrument has a minimum detection limit of 4.0 ppt and has been used in several field campaigns (Xue et al., 2019). The concentrations of NO_2 and NO_x were measured by a nitrogen oxide analyzer (Thermo 42i, Thermo Fisher, USA). Sulfur dioxide (SO_2) was measured by a pulsed fluorescence analyzer (Thermo 43i, Thermo Fisher, USA). Fine particles ($PM_{2.5}$) was measured using an Aerosol Monitor (TSI, Thermo Fisher TEOM 1405). Relative humidity (RH), temperature, wind speed (WS), wind direction (WD), and other metrological data were measured by an automatic weather-monitoring system. Daily atmospheric SO_4^{2-} and NO_3^- samples were collected on the roof of a three-story building on the campus of Tsinghua University in Beijing (40.0° N, 116.3° E) and measured by ion chromatography. Details of the measurements method are described by Ma et al. (2020). The hourly averaged concentrations of the main chemical species of $PM_{2.5}$ were measured by the Gas and Aerosol Compositions Monitor (IGAC, Fortelice International Co., Taiwan) monitoring system (Feng et al., 2018). The observed vertical HONO concentrations from the study of Meng et al.(2020) was measured in December of 2016. The OH measurements in January of 2016 were achieved from the study of Tan et al.(2018).

3 Results and discussions

3.1 Comparison of model prediction with observed HONO

Observed HONO concentrations vary with time, range between 0.04 ppb to 8 ppb, and contains 11 episodes in which the daily peak concentration exceeds 3.3 ppb (Fig. 1a). The high HONO concentration occurs during low wind speeds (Fig. S2). The average HONO concentration during the period is comparable to the reported values for other cities (Table S1). Predicted HONO concentrations obtained with the ORI case are substantially lower than the observed data. In contrast, predicted HONO concentrations obtained with the REV case are substantially higher than those obtained with the ORI case and generally similar to the observed data at night. The ORI case misses the peak values for all

episodes, whereas the REV case captures peak values for most episodes. The observed average concentration during the measurement period is 2.5 ppb, the ORI case only predicts an average concentration of 0.1 ppb, whereas the REV case predicts an average concentration of 2.3 ppb. The NMB of HONO is reduced from -96.5% with the ORI case to -4.8% with the REV case.

Consistent with observations at other cities (Platt et al., 1980; Bernard et al., 2015; Fu et al., 2019), the diurnal variation of observed HONO concentrations in Beijing also reveals higher night-time concentrations than day-time values (Fig. 1b). The predictions with ORI case are an order of magnitude lower than the observed diurnal concentrations. The diurnal variation with the REV case shows a remarkable enhancement of night-time HONO concentrations to levels similar to the observed concentrations. It also increases day-time concentrations, however, predicted values are substantially lower than the observed data, which suggests that additional processes (Oswald et al., 2013; Xing et al., 2017; Romer et al., 2018) are needed to close the gap between observed and predicted day-time HONO concentrations. Night-time and day-time heterogeneous reaction and other updated reactions contribute to the improvement of HONO diurnal pattern. More detailed analysis about this great enhancement is included in section 3.2. The diurnal pattern of the predicted HONO concentrations with the REV agrees better with the observed diurnal pattern.

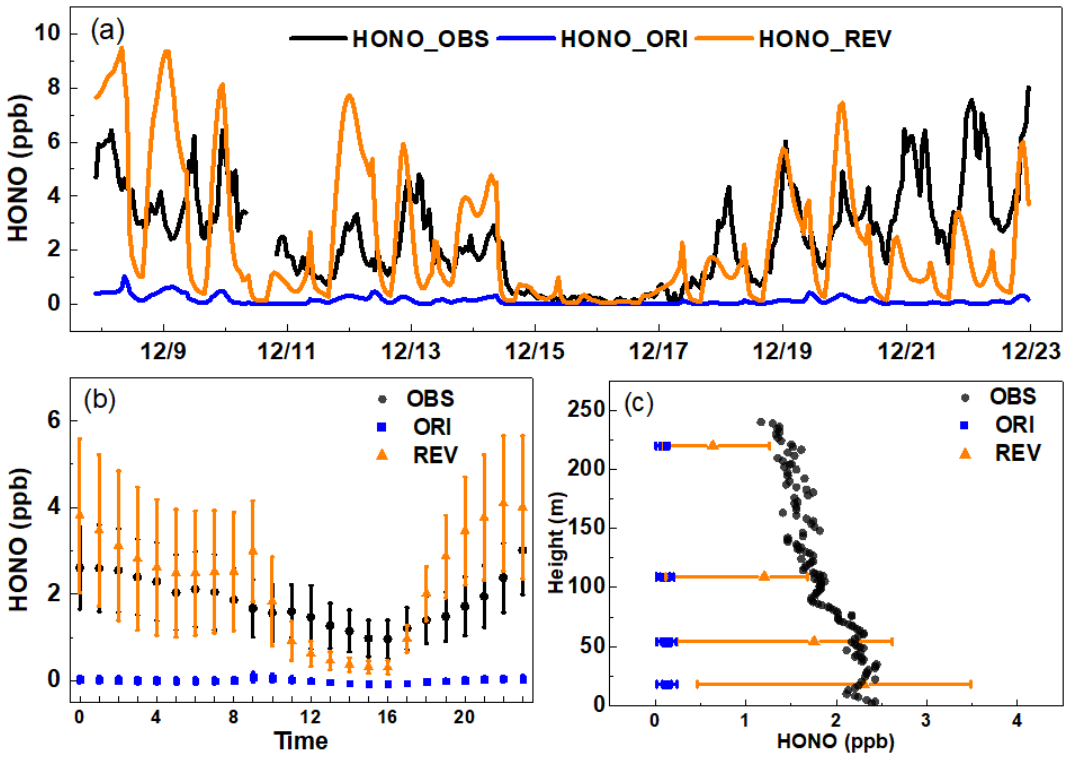

Fig. 1 A comparison of simulated and observed HONO concentrations in Beijing (a) time series (b) diurnal variation, and (c) vertical comparison. Error bars represent 5%-95% values of all HONO concentrations.

We compare predicted vertical distribution with observed vertical HONO concentrations (39.97° N, 116.38° E) from the study of Meng et al.(2020) (Fig. 1c). The measured concentration is the highest at the surface (2.3 ppb), and concentrations decrease with increasing altitude to a value of ~1.2 ppb at ~200 m, which supports the dominant role of the surface HONO production. Predicted HONO levels with ORI case are too small, whereas predictions with the REV agree better with observed data not

only at the surface but also aloft, which provides validity of the simulation results. Consistent with previous HONO vertical concentrations and flux measurements (VandenBoer et al., 2013; Li et al., 2018a), HONO concentration at the surface layer is highest. Model simulated HONO concentrations (Fig. 1c) show a decreasing trend with height similar to the trend in observation data reported by Meng et al.(2020). Model HONO concentrations at upper layers (above 50 m in Fig. 1c) are slightly under-estimated. Model HONO concentrations in these layers are produced mainly by the heterogeneous reaction of NO_2 on aerosol surfaces and the reaction of NO+OH. Aerosol indirect effects can reduce photolysis rate coefficient of HONO (Xing et al., 2017). Decreasing photolysis can improve HONO concentrations in the upper layers in polluted air.

The $HONO/NO_2$ ratio is used as an indicator to estimate the efficiency of heterogeneous NO_2–HONO conversion (Kleffmann et al., 2006; Li et al., 2012). The observed $HONO/NO_2$ ratios ranging between 0.003 and 0.15 are much higher than reported values in the vehicle exhausts (0.001-0.008) which suggests that HONO formation is governed mainly by the secondary production (Kirchstetter et al., 1996; Kurtenbach et al., 2001). The diurnal variation of observed and predicted $HONO/NO_2$ ratios are shown in Fig. S3. The predicted $HONO/NO_2$ ratios increase substantially with REV compared with the ORI case. The average ratio of $HONO/NO_2$ increases from 0.0027 with ORI and to 0.053 with REV, which is in agreement with the observed value of 0.055. The NMB of hourly average simulated $HONO/NO_2$ ratios at night-time decreases from -94.4% with ORI and to -34.2% with REV. The model results suggest that NO_2 heterogeneous conversion is the most important reaction for simulating atmospheric HONO concentrations.

According to our detailed literature review in methodology part, uncertainties of HONO prediction might be largely associated with four key parameters and inputs including the uptake coefficient of NO_2 at ground surface, the aerosol nitrate photolysis rate coefficient, the daytime photolysis rate coefficient, as well as the baseline NO_x emissions. Sensitivity analysis was conducted to examine the influences from those parameters, suggesting that HONO concentration could be doubled with different parameters (see Supplementary Information). Besides, some sources including the photolysis of deposited HNO_3, soil emission and traffic emission could also affect predicted HONO concentration, while the importance of these sources is difficult to quantify. Future studies in improving the accuracy of these parameters are important to reduce the uncertainties of HONO prediction.

3.2 Relative contribution of different HONO reactions

To gain insights into HONO reactions, production rates of different reactions are calculated, and the diurnal variation of the production rates is presented in Fig. S7. The production rates from the heterogeneous reaction on ground surfaces (denoted HONOfrNO2G) are higher during the day than those at night because of the higher rate constant. During night-time (18-5 h / 6:00 p.m.-5:00 a.m.), it dominates the HONO production with an average production rate of 1.4 ppb/h. Similar to HONOfrNO2G, the production rates from the heterogeneous reaction on aerosol surfaces (denoted HONOfrNO2A) are also higher during day-time compared with those at night-time. It contributes an average production rate of 0.2 ppb/h during night-time. The contribution of other reactions to night-time HONO production are relatively small (<0.03ppb/h). During day-time (6-17 h / 6:00 a.m.–5:00 p.m.), HONOfrNO2G also dominates the production with an average contribution of 2.05 ppb/h. HONOfrNO2A is the second most important contributor during day-time with an average production

rate of 0.54 ppb/h. The photolysis of NO_3^- is the third contributor with an average production of 0.04 ppb/h. Gas-phase reactions collectively contribute an average production rate of ~0.41 ppb/h. The NO+OH reaction is the most important gas-phase reaction, producing HONO at an average rate of 0.37 ppb/h. The average day-time production rates of the acid displacement reactions of HNO_3 and HCl are 0.25 ppb/h and 0.03 ppb/h, respectively. The contribution of the reaction on elemental carbon (EC) is even smaller (<0.01 ppb/h). Day-time production from the heterogeneous reaction on ground and aerosol surfaces is greater than the combined production from all other reactions. Although updated day-time reaction rates are higher than that of night-time, accelerated photochemical loss slow down the HONO increase during day-time.

The relative contribution of the chemistry updates to HONO formation (REV) is shown in Fig. 2. HONOfrNO2G is the most important reaction, contributing ~86.2% of night-time HONO production. HONOfrNO2A is the second largest contributor, representing ~12.3% of night-time HONO production. During day-time, HONOfrNO2G contributes ~64.7% of the HONO production, whereas HONOfrNO2A is the second largest contributor, representing 12.6% of the HONO production. Day-time HONO production rate from HONOfrNO2A is higher than that at night-time due to the higher rate constant. Consequently, the relative importance of day-time heterogeneous reaction on aerosol surfaces increases, whereas the relative importance of day-time heterogeneous reaction on ground surfaces decreases. The acid displacement reaction of HNO_3 contributes 11% to day-time HONO formation, and its contribution peaks at 5 p.m. (17 h). The average contribution of gas-phase reactions, photolysis of NO_3^- and acid displacement reactions to day-time HONO production are 9.4%, 1.0%, and 1.3%, respectively. Note that the reaction of OH+NO becomes important in the morning (9 to 10 a.m.) during which it contributes 17.4% of the total HONO production. Averaged over the day and night, HONOfrNO2G is the most significant reaction, contributing 75.6% of the HONO production. HONOfrNO2A is the second largest contributor, representing 12.3% of the HONO production. The gas-phase reactions and the acid displacement reaction of HNO_3 are the third most important contributor each accounting for 5.6% of HONO production. Although HONOfrNO2G had a relatively lower uptake coefficient than the aerosol surface reaction, the reaction rate was large because of the greater ground surface area density (0.047 m^2 m^{-3}) compared with the aerosol surface area density (0.0014 m^2 m^{-3}).

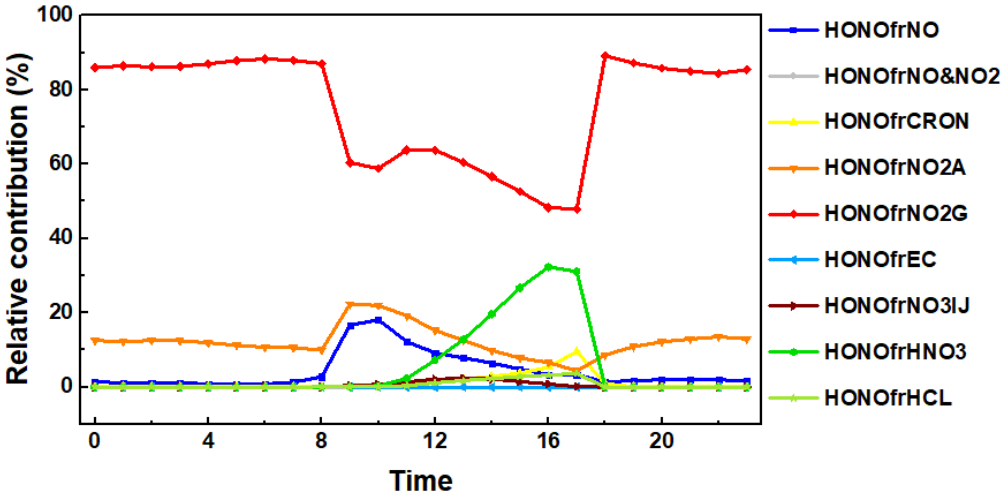

Fig. 2 Relative contribution of different HONO reactions to near-ground-level HONO concentration in Beijing in December. The production from the NO+OH reaction is denoted as HONOfrNO, the production from the NO+NO2+H2O reaction is denoted as HONOfrNO&NO2, the production from cresol is denoted as HONOfrCRON, the production from the heterogeneous reaction on ground surfaces is denoted as HONOfrNO2G, the production from the heterogeneous reaction on aerosol surfaces is denoted as HONOfrNO2A, the production from the reaction of EC is denoted as HONOfrEC, the production from the photolysis of NO_3^- is denoted as HONOfrNO3IJ, the production from the acid displacement reaction of HNO_3 is denoted as HONOfrHNO3, and the production from acid displacement reaction of HCl is denoted as HONOfrHCL.

3.3 Impacts of HONO chemistry on hydroxyl radical concentration

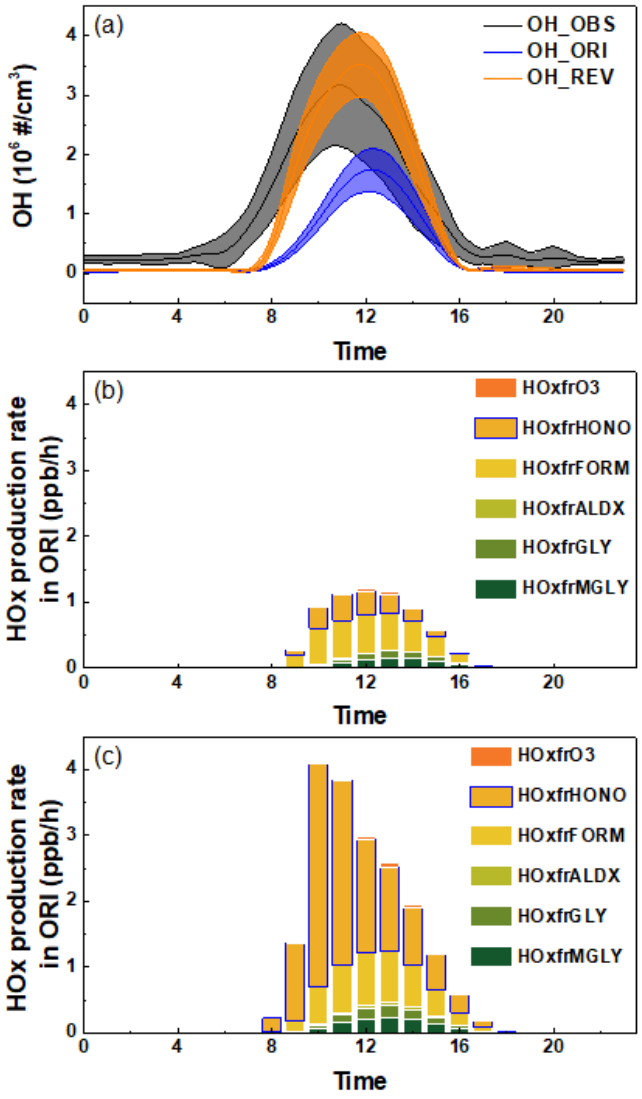

Fig 3 (a) A comparison of simulated and observed diurnal variation of OH. Shadow in Fig. 3a indicates the range of observation. (b) HO_x formation rates from different photolytic reactions with the ORI case and (c) HO_x formation rates from different photolytic reactions with the REV case. The production of HO_x from the O_3 photolysis is denoted as HOxfrO3, the production of HO_x from the HONO photolysis is denoted as HOxfrHONO, the production of HO_x from the formaldehyde photolysis is denoted as HOxfrFORM, the production of HO_x from the higher aldehyde photolysis is denoted as HOxfrALDX, the production of HO_x from the glyoxal photolysis is denoted as HOxfrGLY, and the production of HO_x from the methyl glyoxal photolysis is denoted as HOxfrMGLY.

Enhanced HONO production increases model OH concentration via photolysis. We compare predicted OH concentrations with observed winter data (40.41° N, 116.68 ° E) reported by Tan et al. (2018) in Fig 3a. Observed concentrations are low (~2-3×10^5 /#/cm^3) at night and rapidly increase in the morning reaching a peak value of ~3×10^6 /#/cm^3 at around 11:00 a.m., then slowly decrease to the low nightly values. The ORI case under-predicts the observed peak value by a factor of ~2, and the model peak time occurs 1 to 1.5 hours after the observed peak time, which is consistent with a previous study in

which additional HONO reactions increased OH levels by a factor of >2 (Xue et al., 2020). In addition, the morning enhancement rate with ORI is very low compared with the observed rate. In contrast, the REV case reproduces the observed peak and improves the timing of the peak. The morning enhancement rate also substantially increases and closely tracks the observed enhancement rate. The daily average concentration of OH with REV increases by ~98% compared with that obtained with ORI. Thus, the REV case successfully captures the morning enhancement rate and the peak, and improves the timing of the peak in observed OH data in Beijing. Overall, it captures the observed OH concentration in Beijing much better than the model with the original chemistry. To examine the vertical extent of the impact on OH, predicted OH concentrations with altitude are shown in Fig. S8 (40.0 ° N, 116.3 ° E). Predicted OH concentration with ORI is the lowest at the surface and increases with altitude primarily because of higher O_3 aloft. The REV case increases OH concentration not only due to the surface HONO but also aloft. However, the impact on OH decreases with altitude as the HONO production decreases with altitude.

Various photolytic reactions, including the photolysis of O_3, HONO, formaldehyde, higher aldehyde, glyoxal, and methyl glyoxal, produce HO_x ($OH+HO_2$) are in the model. To understand the relative impacts of these HONO reactions on HO_x production, we compare the diurnal production rates of HO_x from these reactions in Fig. 3b and c. In the ORI case (Fig. 3b), the production of HO_x is relatively small and dominated by the photolysis of HONO and formaldehyde. The photolysis of HONO and formaldehyde start producing HO_x at 9 a.m. which initiates day-time atmospheric chemistry. From late morning, the production of HO_x from glyoxal and methyl glyoxal also contributes to the continuation of day-time atmospheric chemistry. In our simulation, glyoxal and methyl glyoxal originate from the oxidation of aromatics in the atmosphere because isoprene concentration in Beijing is low in winter. Averaged over the entire day, the photolysis of formaldehyde is the largest contributor (0.14 ppb/h) and the photolysis of HONO is the second largest contributor (0.08 ppb/h) to the total HO_x production rate. The production from O_3 and higher aldehyde photolysis are small as their concentrations are low.

In contrast, the HO_x production rates in the REV case are much higher than those in the ORI case because of the enhanced formation from HONO (Fig. 3c). The photolysis of HONO produces HO_x in the morning, which then kick-starts day-time atmospheric chemistry at 8 a.m. (1 h earlier than in the ORI case) and continues to play an important role during the entire day. From late morning, the production of HO_x from formaldehyde, glyoxal, methyl glyoxal, and higher aldehyde also contributes to the continuation of day-time atmospheric chemistry. The production of HO_x from glyoxal, methyl glyoxal, and higher aldehydes plays a larger role compared with that in the ORI case because of higher concentrations produced by the enhanced oxidation of aromatics by higher OH. The photolysis of HONO is the largest contributor (0.5 ppb/h) to the overall HO_x production rate averaged over the entire day while the photolysis of formaldehyde is the second largest contributor (0.18 ppb/h). Thus, HONO plays a crucial role in producing OH in the morning, without updated reactions, the start of day-time atmospheric chemistry is delayed; and the reaction rates are slower, it also plays an important role in atmospheric chemistry throughout the day. Many other photolytic reactions also produce HO_x in the model; however, the productions from the other pathways are small and do not affect our calculation, hence, they are not shown in the figure. The daytime underestimation of HONO in Fig.1 may potentially lead to the underestimation of OH concentration; however, the aerosol indirect effect may lower the OH concentration by reducing the rates of HO_x formation. Therefore, more accurate HONO

simulation needs to consider more complex and significant atmospheric chemical processes.

HONO can affect greatly the daily OH budget (Platt et al., 1980; Harris et al., 1982; Li et al., 2018c; Lu et al., 2019; Xue et al., 2020). Our simulations with the additional HONO reactions enhances OH, which in turn increases HO_2 by the fast conversion between OH and HO_2 radicals (Heard and Pilling, 2003; Lu et al., 2012). The reaction rate of the HO_2+NO reaction increases from 1.8 ppb/h in ORI to 3.6 ppb/h in REV. This indicates that the HONO chemistry also indirectly promotes the formation of OH by increasing the activity of HO_2. This highlights the promoting role of HONO in gas-phase radicals.

Increased OH concentration oxidizes additional volatile organic compounds (VOCs), lowers the concentrations of precursor species, and increases the concentrations of secondary species (Table S3). Enhanced oxidation of VOCs, sulfur dioxide, and NO_2 leads to secondary pollutants, including SO_4^{2-}, NO_3^-, NH_4^+, and SOA, which are discussed in the next section.

3.4 Impacts of HONO chemistry on the formation of secondary particles

Daily averaged model predicted SO_4^{2-}, NO_3^-, and NH_4^+ concentrations are compared with observed data in Beijing in Fig. 4. The ORI case captures the observed trend but generally under-estimates the observed SO_4^{2-} concentrations, whereas the REV case enhances SO_4^{2-} concentrations and closes the gap between model predictions and observation data. Over the entire simulation period, the average concentration of SO_4^{2-} is increased from 13.3 μg/m^3 to 15.8 μg/m^3 (19%). CMAQv5.3 includes six chemical pathways for the conversion of SO_2 into SO_4^{2-} (Sarwar et al., 2011). These are ① the gas-phase oxidation of SO_2 by OH, aqueous-phase oxidation of S(IV) (the sum of $SO_2 \bullet H_2O$ [hydrated SO_2], HSO_3^- [bisulfite ion] and SO_3^{2-} [sulfite ion]) by ② H_2O_2 (hydrogen peroxide), ③ O_3, ④ PAA (peroxyacetic acid), ⑤ MHP (methylhydroperoxide), and ⑥ oxygen catalyzed by the iron (Fe[III]) and manganese (Mn[II]). We utilized the sulfate tracking model to examine SO_4^{2-} production from these chemical pathways over Beijing. The SO_4^{2-} production from the gas-phase oxidation of SO_2 by OH in the REV is ~79% greater than that of the ORI case because of the higher OH concentration from HONO photolysis. SO_4^{2-} production from the aqueous-phase oxidation of S(IV) by H_2O_2 in the ORI is relatively small because the predicted H_2O_2 concentration is also small in winter. However, the REV case enhances H_2O_2 concentration, which consequently also increases the SO_4^{2-} production from this pathway. The other chemical pathways produce similar concentrations in both models, except the oxygen catalyzed by the Fe[III] and Mn[II] pathway, which produce slightly lower SO_4^{2-} production in the REV case because of the competition among different chemical pathways and greater oxidation by the OH initiated pathway.

Table 3. Predicted SO_4^{2-} concentration in Beijing from different chemical pathways in CMAQv5.3

Chemical pathway	Average SO_4^{2-} concentration in ORI (μg/m^3)	Average SO_4^{2-} concentration in REV (μg/m^3)
SO_2 + OH	2.23	3.99
S(IV) + H_2O_2	0.25	0.41

S(IV) + O_3	0.02	0.02
S(IV) + O_2 (TMI)	0.61	0.50
S(IV) + MHP	0.01	0.01
S(IV) + PAA	<0.01	<0.01

501

502 TMI: S(IV) oxidation by oxygen catalyzed by Fe[III] and Mn[II]

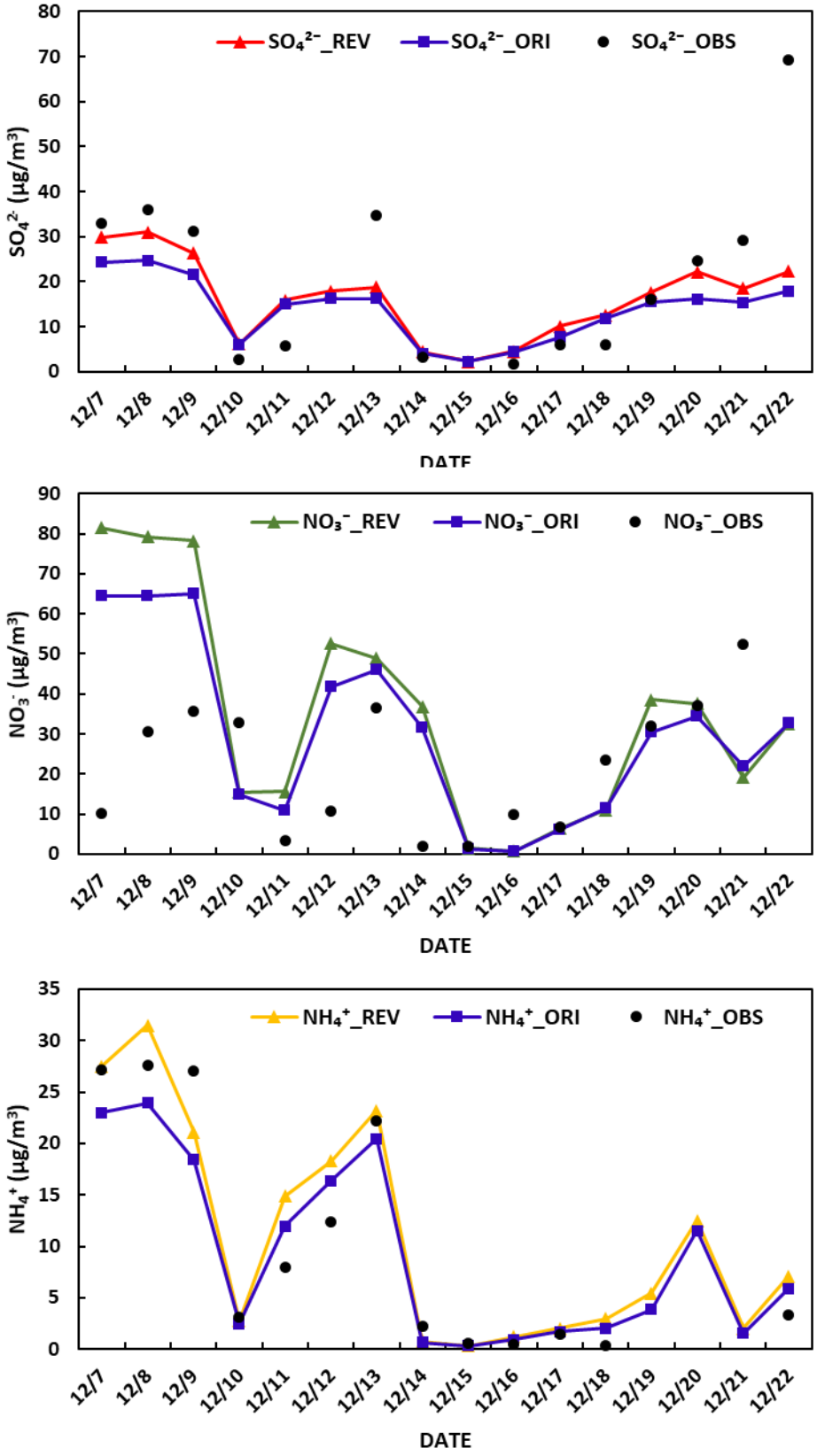

503

504 **Fig. 4 A comparison of simulated and observed daily averaged sulfate, nitrate and ammonium**
505 **concentration in Beijing**

506 Additional SO_4^{2-} production is needed in the model to close the gap between the model prediction and

observed data. Several investigators have proposed other pathways that can generate additional SO_4^{2-} production. For example, Gen et al. (2019) conducted laboratory experiments and reported that the photolysis of NO_3^- can generate N(III) (HONO+NO_2^-) in aerosol liquid water, which oxidizes S(IV) into SO_4^{2-} . Zheng et al. (2020) recently incorporated such a pathway and reported that it can enhance SO_4^{2-} production and can explain 15% to 65% of the gap between model predictions and observed SO_4^{2-} concentrations in China. Shao et al. (2019) implemented several additional heterogeneous SO_4^{2-} formation pathways for oxidation of S(IV) in aerosol liquid water and reported that the pathways can enhance SO_4^{2-} production by 20% in China. Wang et al. (2020) recently reported that S(IV) can be oxidized by HONO and NO_2 in cloud and fog to produce SO_4^{2-} in China. Other investigators (Wang et al., 2016; Ye et al., 2018) have suggested additional chemical pathways for SO_4^{2-} production in China. Additional research is needed to further understand the chemical pathways for SO_4^{2-} production in China (Wang et al., 2020b). These pathways are not the focus of this study and, therefore, are not included in our simulations that leads to the model underpredictions. However, our analysis reveals that the HONO chemistry and the subsequent production of OH can enhance SO_4^{2-} production in China, so should be included in air quality models.

The ORI case has mixed performance in simulating observed NO_3^- (Fig. 4). It over-estimates the daily-averaged observed NO_3^- concentration on some days but captures or under-estimates the observed concentrations on the other. The over-estimation of winter NO_3^- by CMAQ has been reported in previous studies (Yu et al., 2005; Appel et al., 2008). Several reactions contribute to the formation of HNO_3 in CMAQv5.3, which then partitions into NO_3^-. The heterogeneous hydrolysis of N_2O_5 is the most important night-time reaction, and the oxidation of NO_2 by OH is the most important day-time reaction forming HNO_3. CMAQv5.3 uses the parameterization of Davis et al. (2008) for calculating the uptake coefficient for the heterogeneous hydrolysis of N_2O_5. It does not include the organic-coating effect (Anttila et al., 2006; Riemer et al., 2009) that can lower the uptake coefficient. Several studies (Brown et al., 2006; Chang et al., 2016; McDuffie et al., 2018; Wang et al., 2020a) have suggested that the parametrizations used in air quality models, including box model, WRF-CHEM and CMAQv5.3, produce higher uptake coefficients than that derived from observation-based studies. These higher uptake coefficients produce high levels of HNO_3 and NO_3^- in the model. A recent study also suggests that the heterogeneous uptake coefficient in China can be even lower than the values derived over the United States (Wang et al., 2020b). Our current model does not include such lower uptake coefficient and over-predicts NO_3^- concentrations. Our IRR analysis of the ORI case results suggests that 30.3% of NO_3^- (averaged over the entire simulation period in Beijing) is produced via night-time heterogeneous hydrolysis of N_2O_5, and 69.7% is produced via day-time oxidation of NO_2 by OH. The revised chemistry further enhances predicted NO_3^- primarily via the enhanced day-time oxidation of NO_2. Overall, night-time heterogeneous hydrolysis of N_2O_5 contributes 27.6%, and day-time oxidation of NO_2 contributes 72.4% in the REV case. Consequently, predicted NO_3^- concentrations with the revised chemistry further are overestimated on most days.

Because of the increased production of SO_4^{2-} and fNO_3^-, the average concentration of NH_4^+ also increased from 11.1μg/m^3 in ORI and to 13.1μg/m^3 in REV (Fig. 4). NH_4^+ formation is promoted by enhancing the neutralization of sulfuric acid and HNO_3 by ammonia. The dissolution of the precursor and the ion balance is the main factor for the growth of NH_4^+ in CMAQv5.3. The overestimation of NO_3^- leads to the overestimation of NH_4^+ (Liu et al., 2020).

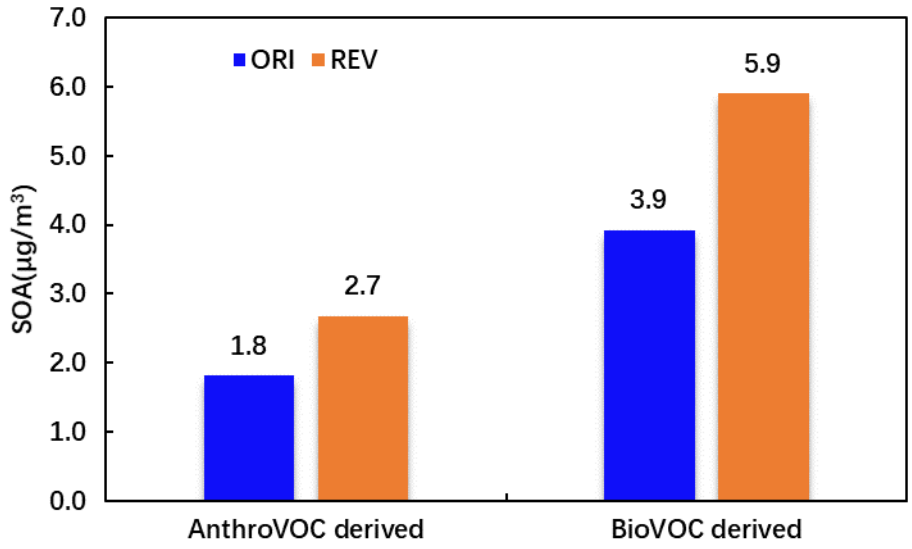

Fig. 5 Predicted monthly average SOA concentration from anthropogenic VOCs (Anthro-VOC-derived) and biogenic VOCs (Bio-VOC-derived) in Beijing. Numbers in this figure only involve SOA from representative anthropogenic or biogenic VOCs.

CMAQv5.3 has a comprehensive treatment of organic aerosols (Murphy et al., 2017; Pye et al., 2017; Xu et al., 2018), including SOA production from anthropogenic-VOC (Anthro-VOC-derived) and biogenic-VOC (Bio-VOC-derived) Fig. 5 displays the Anthro-VOC-derived and Bio-VOC-derived SOA in Beijing.. The REV case enhances the concentration of Anthro-VOC-derived SOA by 0.9 μg/m^3 (50%) and Bio -VOC-derived SOA by 2.0 μg/m^3 (51%). Enhanced OH from additional HONO enhances the oxidation of VOCs (Table S3) and promotes the SOA formation, which also is reported in previous studies. For example, Xing et al. (2019) used the WRF-CHEM model to examine the impact of HONO chemistry updates on SOA formation over the BTH region in winter and reported that the heterogeneous HONO productions can increase the regional average SOA concentration by 46%. Zhang et al. (2019b) implemented six additional HONO reactions (traffic, soil, biomass burning and indoor emissions, and heterogeneous reactions on aerosol and ground surfaces) in the WRF-CHEM model and reported that it successfully reproduced the observed HONO concentrations in Wangdu. They suggested that the additional HONO reactions can increase 2 to 15 μg/m^3 of SOA (meridional-mean) in the BTH region on heavy haze days.

3.5 Spatial impacts on selected species

We examine the spatial impacts of the revised HONO chemistry on selected species (HONO, SO_4^{2-}, NO_3^-, NH_4^+, and SOA) in Fig. 6. Predicted average HONO concentrations with ORI are low (<0.18 ppb) over the entire modeling domain. The revised chemistry increases HONO concentrations over the North China Plain (i.e., BTH, Henan, Shandong) by 0.5 to 3.0 ppb. Abundant emissions of NO_x in this area results in higher NO_2 concentrations, which subsequently enhance HONO concentrations, as the NO_2 reaction on ground is the dominated HONO production source (Fig. 2). It also increases HONO in some other urban areas; however, the impacts in most other areas are relatively small. The ORI case

predicts higher average SO_4^{2-}, NO_3^-, and NH_4^+ concentrations over the North China Plain and the northeast cites. The revised chemistry enhances average of SO_4^{2-} by 1 to 3 μg/m^3, with the maximum enhancements over the south part of the Hebei province. It increases NO_3^- by up to 1.5 μg/m^3 and NH_4^+ by up to 1.1 μg/m^3 over the North China Plain. It also slightly decreases NO_3^- over the North China Plain. The revised HONO chemistry decreases NO_2 concentration while increasing OH concentration. Thus, day-time production of HNO_3 from the NO_2+OH pathway depends on the relative magnitude of the changes of the reaction rate and tends to increase the production in high-NO_x areas while decreasing it in low-NO_x areas. HNO_3 partitions into NO_3^-; thus, changes in HNO_3 production leads to changes in NO_3^- concentration. The ORI case predicts the highest anthropogenic SOA (anthro-SOA) and biogenic SOA (bio-SOA) concentrations over northeast China and the North China Plain. The revised model increases anthro-SOA by 0.37 to 1.2 μg/m^3 over this area and changes bio-SOA over the North China Plain and the northeast cities by -2.0 to 2.3 μg/m^3. Isoprene emissions in some southern cities are relatively higher than in cities in North China Plain in the model. Glyoxal and methylglyoxal generated from isoprene are oxidized by increased OH from the HONO chemistry. SOA derived from biogenic VOC, therefore, is reduced in some areas in Guangdong.

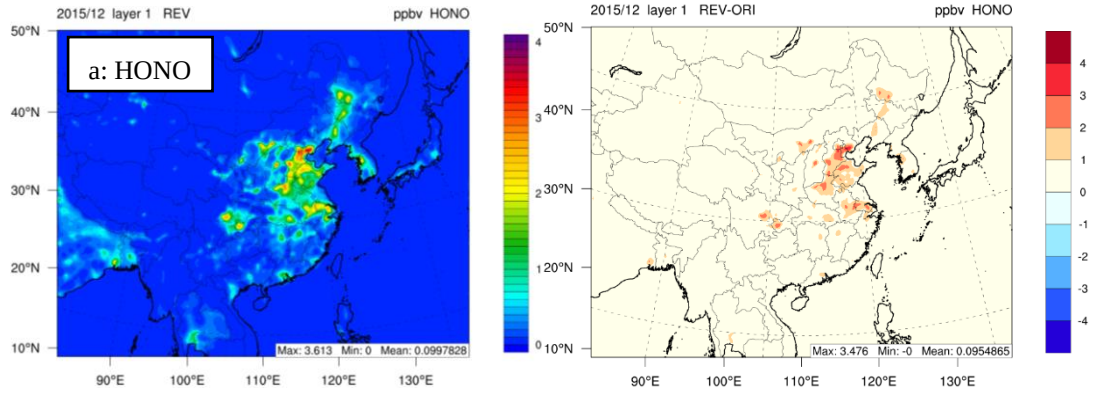

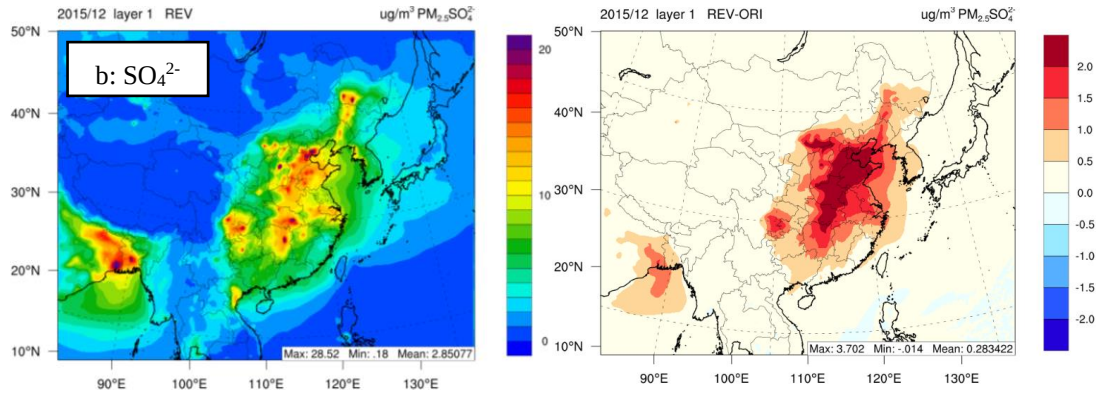

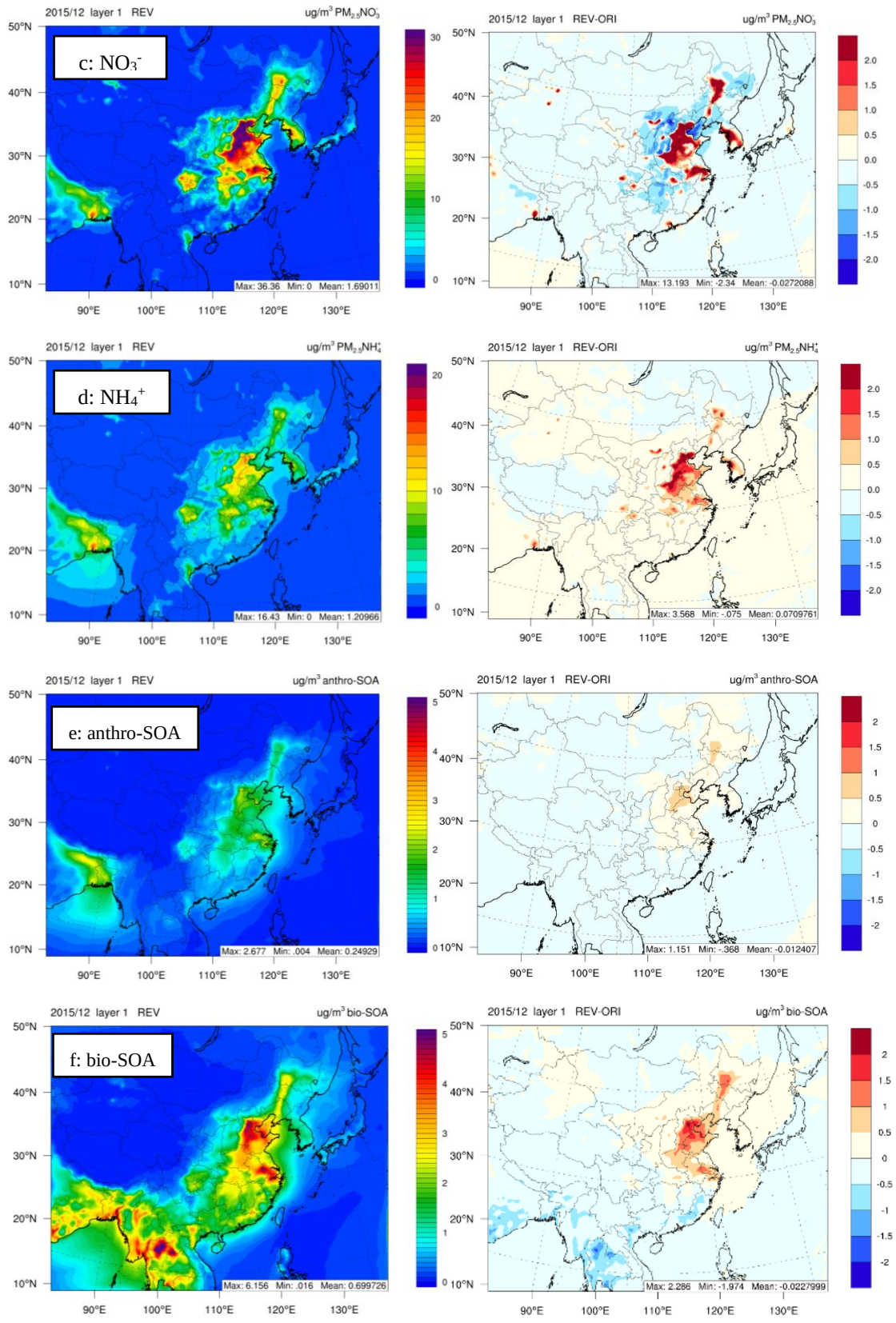

Fig. 6 Spatial distributions of monthly averaged (a) HONO, (b) sulfate, (c) nitrate, (d) ammonium, (e) anthro-VOC-derived SOA, (f) and bio-VOC-derived SOA concentrations simulated with REV and the differences (REV-ORI) between the two simulations in December 2015.

4 Summary

The existing HONO chemistry in CMAQv5.3 cannot re-produce the observed winter HONO concentrations in Beijing. Thus, we revised the HONO chemistry in CMAQv5.3 by implementing several heterogeneous HONO formation pathways. Model predictions with the revised chemistry generally agree with observed HONO concentrations, although the model cannot predict the higher observed day-time concentrations. The heterogeneous production on ground accounts for nearly 75% of the total HONO production. Enhanced HONO increases day-time OH concentrations, which also agree well with observed data in Beijing. Predicted OH concentrations with the existing HONO chemistry are lower than observed data almost by a factor of two. The morning OH enhancement rate is lower than the observed rate, and the timing of the peak is delayed. The revised HONO chemistry improves the morning OH enhancement rate and reproduces the daily peak and the timing of the daily peak. Enhanced OH increases the oxidation rates of SO_2, NO_2, and VOCs in the atmosphere and produces additional secondary pollutants. The revised HONO chemistry moderately enhances SO_4^{2-} concentration in this study. The impact of HONO chemistry on SO_4^{2-} concentration is likely to be greater that shown in this article. For example, HONO chemistry enhances NO_3^-, which, in turn, can produce additional SO_4^{2-} via the photolysis of NO_3^- (Zheng et al., 2020). The oxidation of S(IV) by HONO in cloud and fog also can produce additional SO_4^{2-} (Wang et al., 2020). Such pathways are not the focus this study and are not included in the current model. A recent study (Chen et al., 2019) suggests that HONO also can form on snow-covered ground, which can potentially affect wintertime air quality. Thus, a future study incorporating such chemical reactions to comprehensively examine the impact of HONO chemistry on air quality in different seasons and geographical areas is envisioned.

Code and data availability

The standard CMAQ model is available at: https://www.epa.gov/cmaq. The code changes made in this study and the observational data used in this study are available from the corresponding author upon request (honghe@rcees.ac.cn xingjia@tsinghua.edu.cn).

Author contributions

SPZ initiated the study, carried out analysis, and wrote the initial draft. all authors helped interpret the data, provided feedback, and commented on the manuscript.

Competing interests

The authors declare that they have no conflict of interest.

Acknowledgements

This work was financially supported by the National Natural Science Foundation of China (41877304, 41907190, 51861135102), and the Youth Innovation Promotion Association, CAS (2018060). This work was also financially and technically supported by Toyota Motor Corporation and Toyota Central

Research and Development Laboratories Inc. This work was completed on the “Explorer 100” cluster system of Tsinghua National Laboratory for Information Science and Technology.

Disclaimer

The views expressed in this paper are those of the authors and do not necessarily represent the views or policies of the U.S. EPA.

Reference

An, J., Li, Y., Chen, Y., Li, J., Qu, Y., Tang, Y., 2012. Enhancements of major aerosol components due to additional HONO sources in the North China Plain and implications for visibility and haze. Advances in Atmospheric Sciences 30, 57-66.

Anttila, T., Kiendler-Scharr, A., Tillmann, R., Mentel, T.F., 2006. On the Reactive Uptake of Gaseous Compounds by Organic-Coated Aqueous Aerosols: Theoretical Analysis and Application to the Heterogeneous Hydrolysis of N2O5. The Journal of Physical Chemistry A 110, 10435-10443.

Appel, W., Bhave, P., Gilliland, A., Sarwar, G., Roselle, S., 2008. Evaluation of the community multiscale air quality (CMAQ) model version 4.5: Sensitivities impacting model performance; Part II - particulate matter. Atmospheric Environment 42, 6057-6066.

Bao, F.X., Li, M., Zhang, Y., Chen, C.C., Zhao, J.C., 2018. Photochemical Aging of Beijing Urban PM2.5: HONO Production. Environmental Science & Technology 52, 6309-6316.

Bernard, F., Cazaunau, M., Grosselin, B., Zhou, B., Zheng, J., Liang, P., Zhang, Y., Ye, X., Daële, V., Mu, Y., Zhang, R., Chen, J.-M., Mellouki, A., 2015. Measurements of nitrous acid (HONO) in urban area of Shanghai, China. Environmental Science and Pollution Research 23.

Brown, S.S., Ryerson, T.B., Wollny, A.G., Brock, C.A., Peltier, R., Sullivan, A.P., Weber, R.J., Dubé, W.P., Trainer, M., Meagher, J.F., Fehsenfeld, F.C., Ravishankara, A.R., 2006. Variability in Nocturnal Nitrogen Oxide Processing and Its Role in Regional Air Quality. Science 311, 67.

Byun, D., Schere, K.L., 2006. Review of the governing equations, computational algorithms, and other components of the Models-3 Community Multiscale Air Quality (CMAQ) modeling system. Applied mechanics reviews 59, 51-77.

Chan, W.H., Nordstrom, R.J., Calvert, J.G., Shaw, J.H., 1976a. Kinetic study of nitrous acid formation and decay reactions in gaseous mixtures of nitrous acid, nitrogen oxide (NO), nitrogen oxide (NO2), water, and nitrogen. Environmental Science & Technology 10, 674-682.

Chan, W.H., Nordstrom, R.J., Galvert, J.G., Shaw, J.H., 1976b. An IRFTS spectroscopic study of the kinetics and the mechanism of the reactions in the gaseous system, HONO, NO, NO2, H2O. Chemical Physics Letters 37, 441-446.

Chang, W.L., Brown, S.S., Stutz, J., Middlebrook, A.M., Bahreini, R., Wagner, N.L., Dubé, W.P., Pollack, I.B., Ryerson, T.B., Riemer, N., 2016. Evaluating N2O5 heterogeneous hydrolysis parameterizations for CalNex 2010. Journal of Geophysical Research: Atmospheres 121, 5051-5070.

Chen, Q., Edebeli, J., McNamara, S.M., Kulju, K.D., May, N.W., Bertman, S.B., Thanekar, S., Fuentes, J.D., Pratt, K.A., 2019. HONO, Particulate Nitrite, and Snow Nitrite at a Midlatitude Urban Site during Wintertime. ACS Earth and Space Chemistry 3, 811-822.

Cui, L.L., Li, R., Zhang, Y.C., Meng, Y., Fu, H.B., Chen, J.M., 2018. An observational study of nitrous acid (HONO) in Shanghai, China: The aerosol impact on HONO formation during the haze episodes.

Sci. Total Environ. 630, 1057-1070.
Czader, B.H., Li, X., Rappenglueck, B., 2013. CMAQ modeling and analysis of radicals, radical precursors, and chemical transformations. Journal of Geophysical Research: Atmospheres 118, 11,376-311,387.
Czader, B.H., Rappenglück, B., Percell, P., Byun, D.W., Ngan, F., Kim, S., 2012. Modeling nitrous acid and its impact on ozone and hydroxyl radical during the Texas Air Quality Study 2006. Atmospheric Chemistry and Physics 12, 6939-6951.
Davis, J.M., Bhave, P.V., Foley, K.M., 2008. Parameterization of N2O5 reaction probabilities on the surface of particles containing ammonium, sulfate, and nitrate. Atmos. Chem. Phys. 8, 5295-5311.
Emery, A.E., Muntoni, F., Quinlivan, R.C., 2015. Duchenne muscular dystrophy. OUP Oxford.
Emery, C., Tai, E., Yarwood, G., 2001. Enhanced Meteorological Modeling and Performance Evaluation for Two Texas Ozone Episodes.
Feng, T., Bei, N.F., Zhao, S.Y., Wu, J.R., Li, X., Zhang, T., Cao, J.J., Zhou, W.J., Li, G.H., 2018. Wintertime nitrate formation during haze days in the Guanzhong basin, China: A case study. Environmental pollution 243, 1057-1067.
Finlayson-Pitts, B.J., 2000. Chemistry of the upper and lower atmosphere theory, experiments and applications. San Diego, Calif. : Academic Press, San Diego, Calif.
Fu, X., Wang, T., Zhang, L., Li, Q.Y., Wang, Z., Xia, M., Yun, H., Wang, W.H., Yu, C., Yue, D.L., Zhou, Y., Zheng, J.Y., Han, R., 2019. The significant contribution of HONO to secondary pollutants during a severe winter pollution event in southern China. Atmospheric Chemistry and Physics 19, 1-14.
Gen, M., Zhang, R., Huang, D.D., Li, Y., Chan, C.K., 2019. Heterogeneous SO2 Oxidation in Sulfate Formation by Photolysis of Particulate Nitrate. Environmental Science & Technology Letters 6, 86-91.
Guo, S., Hu, M., Zamora, M.L., Peng, J., Shang, D., Zheng, J., Du, Z., Wu, Z., Shao, M., Zeng, L., Molina, M.J., Zhang, R., 2014. Elucidating severe urban haze formation in China. Proceedings of the National Academy of Sciences 111, 17373-17378.
Harris, G.W., Carter, W.P.L., Winer, A.M., Pitts, J.N., Platt, U., Perner, D., 1982. Observations of nitrous acid in the Los Angeles atmosphere and implications for predictions of ozone-precursor relationships. Environmental Science & Technology 16, 414-419.
He, H., Wang, Y., Ma, Q., Ma, J., Chu, B., Ji, D., Tang, G., Liu, C., Zhang, H., Hao, J., 2014. Mineral dust and NOx promote the conversion of SO2 to sulfate in heavy pollution days. Scientific Reports 4.
Heard, D.E., Pilling, M.J., 2003. Measurement of OH and HO2 in the Troposphere. Chemical reviews 103, 5163-5198.
Huang, L., Zhao, Y., Li, H., Chen, Z., 2015. Kinetics of Heterogeneous Reaction of Sulfur Dioxide on Authentic Mineral Dust: Effects of Relative Humidity and Hydrogen Peroxide. Environmental Science & Technology 49, 10797-10805.
Huang, R.-J., Zhang, Y., Bozzetti, C., Ho, K.-F., Cao, J.-J., Han, Y., Daellenbach, K.R., Slowik, J.G., Platt, S.M., Canonaco, F., 2014. High secondary aerosol contribution to particulate pollution during haze events in China. Nature 514, 218-222.
Jaeglé, L., Shah, V., Thornton, J.A., Lopez-Hilfiker, F.D., Lee, B.H., McDuffie, E.E., Fibiger, D., Brown, S.S., Veres, P., Sparks, T.L., Ebben, C.J., Wooldridge, P.J., Kenagy, H.S., Cohen, R.C., Weinheimer, A.J., Campos, T.L., Montzka, D.D., Digangi, J.P., Wolfe, G.M., Hanisco, T., Schroder, J.C., Campuzano-Jost, P., Day, D.A., Jimenez, J.L., Sullivan, A.P., Guo, H., Weber, R.J., 2018. Nitrogen Oxides Emissions, Chemistry, Deposition, and Export Over the Northeast United States During the WINTER Aircraft Campaign. Journal of Geophysical Research: Atmospheres 123, 12,368-312,393.

Kaiser, E.W., Wu, C.H., 1977. A kinetic study of the gas phase formation and decomposition reactions of nitrous acid. The Journal of Physical Chemistry 81, 1701-1706.
Karamchandani, P., Emery, C., Yarwood, G., Lefer, B., Stutz, J., Couzo, E., Vizuete, W., 2015. Implementation and refinement of a surface model for heterogeneous HONO formation in a 3-D chemical transport model. Atmospheric Environment 112, 356-368.
Kirchstetter, T.W., Harley, R.A., Littlejohn, D., 1996. Measurement of nitrous acid in motor vehicle exhaust. Environmental science & technology 30, 2843-2849.
Kleffmann, J., Gavriloaiei, T., Hofzumahaus, A., Holland, F., Koppmann, R., Rupp, L., Schlosser, E., Siese, M., Wahner, A., 2005. Daytime formation of nitrous acid: A major source of OH radicals in a forest. Geophysical Research Letters 32.
Kleffmann, J., Lörzer, J., Wiesen, P., Kern, C., Trick, S., Volkamer, R., Rodenas, M., Wirtz, K., 2006. Intercomparison of the DOAS and LOPAP techniques for the detection of nitrous acid (HONO). Atmospheric Environment 40, 3640-3652.
Kulmala, M., 2018. Build a global Earth observatory. Nature 553, 21-23.
Kurtenbach, R., Becker, K., Gomes, J., Kleffmann, J., Lörzer, J., Spittler, M., Wiesen, P., Ackermann, R., Geyer, A., Platt, U., 2001. Investigations of emissions and heterogeneous formation of HONO in a road traffic tunnel. Atmospheric Environment 35, 3385-3394.
Lelieveld, J., Evans, J.S., Fnais, M., Giannadaki, D., Pozzer, A., 2015. The contribution of outdoor air pollution sources to premature mortality on a global scale. Nature 525, 367-371.
Li, D.D., Xue, L.K., Wen, L., Wang, X.F., Chen, T.S., Mellouki, A., Chen, J.M., Wang, W.X., 2018a. Characteristics and sources of nitrous acid in an urban atmosphere of northern China: Results from 1-yr continuous observations. Atmospheric Environment 182, 296-306.
Li, G., Bei, N., Cao, J., Huang, R., Wu, J., Feng, T., Wang, Y., Liu, S., Zhang, Q., Tie, X., Molina, L.T., 2017. A possible pathway for rapid growth of sulfate during haze days in China. Atmospheric Chemistry and Physics 17, 3301-3316.
Li, G., Lei, W., Zavala, M., Volkamer, R., Dusanter, S., Stevens, P., Molina, L.T., 2010. Impacts of HONO sources on the photochemistry in Mexico City during the MCMA-2006/MILAGO Campaign. Atmos. Chem. Phys. 10, 6551-6567.
Li, L., Duan, Z., Li, H., Zhu, C., Henkelman, G., Francisco, J.S., Zeng, X.C., 2018b. Formation of HONO from the NH3-promoted hydrolysis of NO2 dimers in the atmosphere. Proceedings of the National Academy of Sciences of the United States of America 115, 7236-7241.
Li, L.J., Hoffmann, M.R., Colussi, A.J., 2018c. Role of Nitrogen Dioxide in the Production of Sulfate during Chinese Haze-Aerosol Episodes. Environmental Science & Technology 52, 2686-2693.
Li, M., Su, H., Li, G., Ma, N., Pöschl, U., Cheng, Y., 2019. Relative importance of gas uptake on aerosol and ground surfaces characterized by equivalent uptake coefficients. Atmospheric Chemistry and Physics 19, 10981-11011.
Li, X., Brauers, T., Häseler, R., Bohn, B., Fuchs, H., Hofzumahaus, A., Holland, F., Lou, S., Lu, K.D., Rohrer, F., Hu, M., Zeng, L.M., Zhang, Y.H., Garland, R.M., Su, H., Nowak, A., Wiedensohler, A., Takegawa, N., Shao, M., Wahner, A., 2012. Exploring the atmospheric chemistry of nitrous acid (HONO) at a rural site in Southern China. Atmospheric Chemistry and Physics 12, 1497-1513.
Liu, Y., Lu, K., Li, X., Dong, H., Tan, Z., Wang, H., Zou, Q., Wu, Y., Zeng, L., Hu, M., Min, K.-E., Kecorius, S., Wiedensohler, A., Zhang, Y., 2019. A Comprehensive Model Test of the HONO Sources Constrained to Field Measurements at Rural North China Plain. Environmental Science & Technology 53, 3517-3525.

Liu, Y., Zhang, Y., Lian, C., Yan, C., Feng, Z., Zheng, F., Fan, X., Chen, Y., Wang, W., Chu, B., 2020. The promotion effect of nitrous acid on aerosol formation in wintertime in Beijing: the possible contribution of traffic-related emissions. Atmospheric Chemistry and Physics 20, 13023-13040.
Liu, Z., Wang, Y., Costabile, F., Amoroso, A., Zhao, C., Huey, L.G., Stickel, R., Liao, J., Zhu, T., 2014. Evidence of Aerosols as a Media for Rapid Daytime HONO Production over China. Environmental Science & Technology 48, 14386-14391.
Lu, K., Fuchs, H., Hofzumahaus, A., Tan, Z., Wang, H., Zhang, L., Schmitt, S.H., Rohrer, F., Bohn, B., Broch, S., Dong, H., Gkatzelis, G.I., Hohaus, T., Holland, F., Li, X., Liu, Y., Liu, Y., Ma, X., Novelli, A., Schlag, P., Shao, M., Wu, Y., Wu, Z., Zeng, L., Hu, M., Kiendler-Scharr, A., Wahner, A., Zhang, Y., 2019. Fast Photochemistry in Wintertime Haze: Consequences for Pollution Mitigation Strategies. Environmental Science & Technology 53, 10676-10684.
Lu, K.D., Rohrer, F., Holland, F., Fuchs, H., Bohn, B., Brauers, T., Chang, C.C., Häseler, R., Hu, M., Kita, K., Kondo, Y., Li, X., Lou, S.R., Nehr, S., Shao, M., Zeng, L.M., Wahner, A., Zhang, Y.H., Hofzumahaus, A., 2012. Observation and modelling of OH and HO₂ concentrations in the Pearl River Delta 2006: a missing OH source in a VOC rich atmosphere. Atmospheric Chemistry and Physics 12, 1541-1569.
Lu, X.C., Wang, Y.H., Li, J.F., Shen, L., Fung, J.C.H., 2018. Evidence of heterogeneous HONO formation from aerosols and the regional photochemical impact of this HONO source. Environ. Res. Lett. 13, 12.
Ma, T., Furutani, H., Duan, F., Kimoto, T., Jiang, J.K., Zhang, Q., Xu, X.B., Wang, Y., Gao, J., Geng, G.N., Li, M., Song, S.J., Ma, Y.L., Che, F., Wang, J., Zhu, L.D., Huang, T., Toyoda, M., He, K.B., 2020. Contribution of hydroxymethanesulfonate (HMS) to severe winter haze in the North China Plain. Atmospheric Chemistry and Physics 20, 5887-5897.
Mathur, R., Roselle, S., Pouliot, G., Sarwar, G., 2008. Diagnostic analysis of the three-dimensional sulfur distributions over the eastern United states using the CMAQ model and measurements from the ICARTT field experiment, Air Pollution Modeling and Its Application XIX. Springer, pp. 496-504.
McDuffie, E.E., Fibiger, D.L., Dubé, W.P., Lopez-Hilfiker, F., Lee, B.H., Thornton, J.A., Shah, V., Jaeglé, L., Guo, H., Weber, R.J., Michael Reeves, J., Weinheimer, A.J., Schroder, J.C., Campuzano-Jost, P., Jimenez, J.L., Dibb, J.E., Veres, P., Ebben, C., Sparks, T.L., Wooldridge, P.J., Cohen, R.C., Hornbrook, R.S., Apel, E.C., Campos, T., Hall, S.R., Ullmann, K., Brown, S.S., 2018. Heterogeneous N2O5 Uptake During Winter: Aircraft Measurements During the 2015 WINTER Campaign and Critical Evaluation of Current Parameterizations. Journal of Geophysical Research: Atmospheres 123, 4345-4372.
Meng, F., Qin, M., Tang, K., Duan, J., Fang, W., Liang, S., Ye, K., Xie, P., Sun, Y., Xie, C., Ye, C., Fu, P., Liu, J., Liu, W., 2020. High-resolution vertical distribution and sources of HONO and NO₂ in the nocturnal boundary layer in urban Beijing, China. Atmospheric Chemistry and Physics 20, 5071-5092.
Monge, M., D'Anna, B., Mazri, L., Giroir-Fendler, A., Ammann, M., Donaldson, D.J., George, C., 2010. Light changes the atmospheric reactivity of soot. Proceedings of the National Academy of Sciences of the United States of America 107, 6605-6609.
Murphy, B.N., Woody, M.C., Jimenez, J.L., Carlton, A.M.G., Hayes, P.L., Liu, S., Ng, N.L., Russell, L.M., Setyan, A., Xu, L., Young, J., Zaveri, R.A., Zhang, Q., Pye, H.O.T., 2017. Semivolatile POA and parameterized total combustion SOA in CMAQv5.2: impacts on source strength and partitioning. Atmos. Chem. Phys. 17, 11107-11133.

Oswald, R., Behrendt, T., Ermel, M., Wu, D., Su, H., Cheng, Y., Breuninger, C., Moravek, A., Mougin, E., Delon, C., 2013. HONO emissions from soil bacteria as a major source of atmospheric reactive nitrogen. Science 341, 1233-1235.

Platt, U., Perner, D., Harris, G.W., Winer, A.M., Pitts, J.N., 1980. Observations of nitrous acid in an urban atmosphere by differential optical absorption. Nature 285, 312-314.

Pye, H.O.T., Murphy, B.N., Xu, L., Ng, N.L., Carlton, A.G., Guo, H., Weber, R., Vasilakos, P., Appel, K.W., Budisulistiorini, S.H., Surratt, J.D., Nenes, A., Hu, W., Jimenez, J.L., Isaacman-VanWertz, G., Misztal, P.K., Goldstein, A.H., 2017. On the implications of aerosol liquid water and phase separation for organic aerosol mass. Atmos. Chem. Phys. 17, 343-369.

Quan, J., Tie, X., Zhang, Q., Liu, Q., Li, X., Gao, Y., Zhao, D., 2014. Characteristics of heavy aerosol pollution during the 2012–2013 winter in Beijing, China. Atmospheric Environment 88, 83-89.

Rasool, Q.Z., Bash, J.O., Cohan, D.S., 2019. Mechanistic representation of soil nitrogen emissions in the Community Multiscale Air Quality (CMAQ) model v 5.1. Geosci Model Dev 12, 849-878.

Riemer, N., Vogel, H., Vogel, B., Anttila, T., Kiendler-Scharr, A., Mentel, T.F., 2009. Relative importance of organic coatings for the heterogeneous hydrolysis of N2O5 during summer in Europe. Journal of Geophysical Research: Atmospheres 114.

Romer, P.S., Wooldridge, P.J., Crounse, J.D., Kim, M.J., Wennberg, P.O., Dibb, J.E., Scheuer, E., Blake, D.R., Meinardi, S., Brosius, A.L., Thames, A.B., Miller, D.O., Brune, W.H., Hall, S.R., Ryerson, T.B., Cohen, R.C., 2018. Constraints on Aerosol Nitrate Photolysis as a Potential Source of HONO and NOx. Environmental Science & Technology 52, 13738-13746.

Sarwar, G., Fahey, K., Napelenok, S., Roselle, S., Mathur, R., 2011. Examining the impact of CMAQ model updates on aerosol sulfate predictions, The 10th Annual CMAS Models-3 User's Conference, October, Chapel Hill, NC.

Sarwar, G., Roselle, S.J., Mathur, R., Appel, W., Dennis, R.L., Vogel, B., 2008. A comparison of CMAQ HONO predictions with observations from the northeast oxidant and particle study. Atmospheric Environment 42, 5760-5770.

Shao, J., Chen, Q., Wang, Y., Lu, X., He, P., Sun, Y., Shah, V., Martin, R.V., Philip, S., Song, S., Zhao, Y., Xie, Z., Zhang, L., Alexander, B., 2019. Heterogeneous sulfate aerosol formation mechanisms during wintertime Chinese haze events: air quality model assessment using observations of sulfate oxygen isotopes in Beijing. Atmos. Chem. Phys. 19, 6107-6123.

Skamarock, W.C., Klemp, J.B., 2008. A time-split nonhydrostatic atmospheric model for weather research and forecasting applications. Journal of computational physics 227, 3465-3485.

Spataro, F., Ianniello, A., 2014. Sources of atmospheric nitrous acid: State of the science, current research needs, and future prospects. J. Air Waste Manage. Assoc. 64, 1232-1250.

Spataro, F., Ianniello, A., Esposito, G., Allegrini, I., Zhu, T., Hu, M., 2013. Occurrence of atmospheric nitrous acid in the urban area of Beijing (China). Sci. Total Environ. 447, 210-224.

Stemmler, K., Ammann, M., Donders, C., Kleffmann, J., George, C., 2006. Photosensitized reduction of nitrogen dioxide on humic acid as a source of nitrous acid. Nature 440, 195-198.

Stutz, J., Alicke, B., Neftel, A., 2002. Nitrous acid formation in the urban atmosphere: Gradient measurements of NO2 and HONO over grass in Milan, Italy. Journal of Geophysical Research: Atmospheres 107, LOP 5-1-LOP 5-15.

Su, H., Cheng, Y., Oswald, R., Behrendt, T., Trebs, I., Meixner, F.X., Andreae, M.O., Cheng, P., Zhang, Y., Pöschl, U., 2011. Soil Nitrite as a Source of Atmospheric HONO and OH Radicals. Science 333, 1616.

Sun, Y., Wang, Z., Fu, P., Jiang, Q., Yang, T., Li, J., Ge, X., 2013. The impact of relative humidity on aerosol composition and evolution processes during wintertime in Beijing, China. Atmospheric Environment 77, 927-934.

Tan, Z., Rohrer, F., Lu, K., Ma, X., Bohn, B., Broch, S., Dong, H., Fuchs, H., Gkatzelis, G.I., Hofzumahaus, A., Holland, F., Li, X., Liu, Y., Liu, Y., Novelli, A., Shao, M., Wang, H., Wu, Y., Zeng, L., Hu, M., Kiendler-Scharr, A., Wahner, A., Zhang, Y., 2018. Wintertime photochemistry in Beijing: observations of ROx radical concentrations in the North China Plain during the BEST-ONE campaign. Atmos. Chem. Phys. 18, 12391-12411.

Tong, S., Hou, S., Zhang, Y., Chu, B., Liu, Y., He, H., Zhao, P., Ge, M., 2016. Exploring the nitrous acid (HONO) formation mechanism in winter Beijing: direct emissions and heterogeneous production in urban and suburban areas. Faraday discussions 189, 213-230.

Tsona, N.T., Du, L., 2019. A potential source of atmospheric sulfate from O2−-induced SO2 oxidation by ozone. Atmos. Chem. Phys. 19, 649-661.

VandenBoer, T.C., Brown, S.S., Murphy, J.G., Keene, W.C., Young, C.J., Pszenny, A.A.P., Kim, S., Warneke, C., de Gouw, J.A., Maben, J.R., Wagner, N.L., Riedel, T.P., Thornton, J.A., Wolfe, D.E., Dubé, W.P., Öztürk, F., Brock, C.A., Grossberg, N., Lefer, B., Lerner, B., Middlebrook, A.M., Roberts, J.M., 2013. Understanding the role of the ground surface in HONO vertical structure: High resolution vertical profiles during NACHTT-11. Journal of Geophysical Research: Atmospheres 118, 10,155-110,171.

VandenBoer, T.C., Young, C.J., Talukdar, R.K., Markovic, M.Z., Brown, S.S., Roberts, J.M., Murphy, J.G., 2015. Nocturnal loss and daytime source of nitrous acid through reactive uptake and displacement. Nature Geoscience 8, 55-60.

Vogel, B., Vogel, H., Kleffmann, J., Kurtenbach, R., 2003. Measured and simulated vertical profiles of nitrous acid—Part II. Model simulations and indications for a photolytic source. Atmospheric Environment 37, 2957-2966.

Voogt, J.A., Oke, T.R., 1997. Complete Urban Surface Temperatures. Journal of Applied Meteorology 36, 1117-1132.

Wang, G., Cheng, S., Wei, W., Yang, X., Wang, X., Jia, J., Lang, J., Lv, Z., 2017. Characteristics and emission-reduction measures evaluation of PM2.5 during the two major events: APEC and Parade. The Science of the total environment 595, 81-92.

Wang, G., Zhang, R., Gomez, M.E., Yang, L., Levy Zamora, M., Hu, M., Lin, Y., Peng, J., Guo, S., Meng, J., Li, J., Cheng, C., Hu, T., Ren, Y., Wang, Y., Gao, J., Cao, J., An, Z., Zhou, W., Li, G., Wang, J., Tian, P., Marrero-Ortiz, W., Secrest, J., Du, Z., Zheng, J., Shang, D., Zeng, L., Shao, M., Wang, W., Huang, Y., Wang, Y., Zhu, Y., Li, Y., Hu, J., Pan, B., Cai, L., Cheng, Y., Ji, Y., Zhang, F., Rosenfeld, D., Liss, P.S., Duce, R.A., Kolb, C.E., Molina, M.J., 2016. Persistent sulfate formation from London Fog to Chinese haze. Proceedings of the National Academy of Sciences of the United States of America.

Wang, H., Chen, X., Lu, K., Tan, Z., Ma, X., Wu, Z., Li, X., Liu, Y., Shang, D., Wu, Y., Zeng, L., Hu, M., Schmitt, S., Kiendler-Scharr, A., Wahner, A., Zhang, Y., 2020a. Wintertime N2O5 uptake coefficients over the North China Plain. Science Bulletin 65, 765-774.

Wang, J., Li, J., Ye, J., Zhao, J., Wu, Y., Hu, J., Liu, D., Nie, D., Shen, F., Huang, X., Huang, D.D., Ji, D., Sun, X., Xu, W., Guo, J., Song, S., Qin, Y., Liu, P., Turner, J.R., Lee, H.C., Hwang, S., Liao, H., Martin, S.T., Zhang, Q., Chen, M., Sun, Y., Ge, X., Jacob, D.J., 2020b. Fast sulfate formation from oxidation of SO2 by NO2 and HONO observed in Beijing haze. Nature Communications 11, 2844.

Wang, L.W., Wen, L., Xu, C.H., Chen, J.M., Wang, X.F., Yang, L.X., Wang, W.X., Yang, X., Sui, X.,

Yao, L., Zhang, Q.Z., 2015. HONO and its potential source particulate nitrite at an urban site in North China during the cold season. Sci. Total Environ. 538, 93-101.
Wesely, M., 2007. Parameterization of surface resistances to gaseous dry deposition in regional-scale numerical models. Atmospheric Environment 41, 52-63.
Wesely, M.L., 1989. Parameterization of surface resistances to gaseous dry deposition in regional-scale numerical models. Atmospheric Environment (1967) 23, 1293-1304.
Xing, J., Mathur, R., Pleim, J., Hogrefe, C., Gan, C.M., Wong, D.C., Wei, C., Wang, J.D., 2015. Air pollution and climate response to aerosol direct radiative effects: A modeling study of decadal trends across the northern hemisphere. J. Geophys. Res.-Atmos. 120, 16.
Xing, J., Wang, J., Mathur, R., Wang, S., Sarwar, G., Pleim, J., Hogrefe, C., Zhang, Y., Jiang, J., Wong, D.C., Hao, J., 2017. Impacts of aerosol direct effects on tropospheric ozone through changes in atmospheric dynamics and photolysis rates. Atmospheric Chemistry and Physics 17, 9869-9883.
Xing, L., Wu, J., Elser, M., Tong, S., Liu, S., Li, X., Liu, L., Cao, J., Zhou, J., El-Haddad, I., Huang, R., Ge, M., Tie, X., Prévôt, A.S.H., Li, G., 2019. Wintertime secondary organic aerosol formation in Beijing–Tianjin–Hebei (BTH): contributions of HONO sources and heterogeneous reactions. Atmos. Chem. Phys. 19, 2343-2359.
Xu, K.-M., Krueger, S.K., 1991. Evaluation of Cloudiness Parameterizations Using a Cumulus Ensemble Model. Monthly Weather Review 119, 342-367.
Xu, K.-M., Randall, D.A., 1996. Evaluation of Statistically Based Cloudiness Parameterizations Used in Climate Models. Journal of Atmospheric Sciences 53, 3103-3119.
Xu, L., Pye, H.O.T., He, J., Chen, Y., Murphy, B.N., Ng, N.L., 2018. Experimental and model estimates of the contributions from biogenic monoterpenes and sesquiterpenes to secondary organic aerosol in the southeastern United States. Atmos. Chem. Phys. 18, 12613-12637.
Xu, W., Kuang, Y., Zhao, C., Tao, J., Zhao, G., Bian, Y., Yang, W., Yu, Y., Shen, C., Liang, L., 2019. NH3-promoted hydrolysis of NO2 induces explosive growth in HONO. Atmospheric Chemistry and Physics 19, 10557-10570.
Xue, C., Ye, C., Ma, Z., Liu, P., Zhang, Y., Zhang, C., Tang, K., Zhang, W., Zhao, X., Wang, Y., Song, M., Liu, J., Duan, J., Qin, M., Tong, S., Ge, M., Mu, Y., 2019. Development of stripping coil-ion chromatograph method and intercomparison with CEAS and LOPAP to measure atmospheric HONO. Sci. Total Environ. 646, 187-195.
Xue, C., Zhang, C., Ye, C., Liu, P., Catoire, V., Krysztofiak, G., Chen, H., Ren, Y., Zhao, X., Wang, J., Zhang, F., Zhang, C., Zhang, J., An, J., Wang, T., Chen, J., Kleffmann, J., Mellouki, A., Mu, Y., 2020. HONO budget and its role in nitrate formation in the rural North China Plain. Environmental Science & Technology.
Ye, C., Gao, H., Zhang, N., Zhou, X., 2016. Photolysis of Nitric Acid and Nitrate on Natural and Artificial Surfaces. Environmental Science & Technology 50, 3530-3536.
Ye, C., Liu, P., Ma, Z., Xue, C., Zhang, C., Zhang, Y., Liu, J., Liu, C., Sun, X., Mu, Y., 2018. High H2O2 concentrations observed during haze periods during the winter in Beijing: Importance of H2O2 oxidation in sulfate formation. Environmental Science & Technology Letters 5, 757-763.
Ye, C., Zhang, N., Gao, H., Zhou, X., 2017. Photolysis of Particulate Nitrate as a Source of HONO and NOx. Environmental Science & Technology 51, 6849-6856.
Yu, S., Dennis, R., Roselle, S., Nenes, A., Walker, J., Eder, B., Schere, K., Swall, J., Robarge, W., 2005. An assessment of the ability of three-dimensional air quality models with current thermodynamic equilibrium models to predict aerosol NO3−. Journal of Geophysical Research 110.

Zhang, J., Chen, J., Xue, C., Chen, H., Zhang, Q., Liu, X., Mu, Y., Guo, Y., Wang, D., Chen, Y., Li, J., Qu, Y., An, J., 2019a. Impacts of six potential HONO sources on HOx budgets and SOA formation during a wintertime heavy haze period in the North China Plain. Sci. Total Environ. 681, 110-123.

Zhang, J.W., An, J.L., Qu, Y., Liu, X.G., Chen, Y., 2019b. Impacts of potential HONO sources on the concentrations of oxidants and secondary organic aerosols in the Beijing-Tianjin-Hebei region of China. Sci. Total Environ. 647, 836-852.

Zhang, S., Xing, J., Sarwar, G., Ge, Y., He, H., Duan, F., Zhao, Y., He, K., Zhu, L., Chu, B., 2019c. Parameterization of heterogeneous reaction of SO2 to sulfate on dust with coexistence of NH3 and NO2 under different humidity conditions. Atmospheric Environment 208, 133-140.

Zhang, W.Q., Tong, S.R., Ge, M.F., An, J.L., Shi, Z.B., Hou, S.Q., Xia, K.H., Qu, Y., Zhang, H.X., Chu, B.W., Sun, Y.L., He, H., 2019d. Variations and sources of nitrous acid (HONO) during a severe pollution episode in Beijing in winter 2016. Sci. Total Environ. 648, 253-262.

Zhao, B., Zheng, H., Wang, S., Smith, K.R., Lu, X., Aunan, K., Gu, Y., Wang, Y., Ding, D., Xing, J., Fu, X., Yang, X., Liou, K.-N., Hao, J., 2018. Change in household fuels dominates the decrease in PM_{2.5} exposure and premature mortality in China in 2005–2015. Proceedings of the National Academy of Sciences 115, 12401.

Zheng, B., Zhang, Q., Zhang, Y., He, K.B., Wang, K., Zheng, G.J., Duan, F.K., Ma, Y.L., Kimoto, T., 2015. Heterogeneous chemistry: a mechanism missing in current models to explain secondary inorganic aerosol formation during the January 2013 haze episode in North China. Atmospheric Chemistry and Physics 15, 2031-2049.

Zheng, H., Zhao, B., Wang, S., Wang, T., Ding, D., Chang, X., Liu, K., Xing, J., Dong, Z., Aunan, K., Liu, T., Wu, X., Zhang, S., Wu, Y., 2019. Transition in source contributions of PM2.5 exposure and associated premature mortality in China during 2005–2015. Environment International 132, 105111.

Zhou, X., Gao, H., He, Y., Huang, G., Bertman, S.B., Civerolo, K., Schwab, J., 2003. Nitric acid photolysis on surfaces in low-NOx environments: Significant atmospheric implications. Geophysical Research Letters 30.

U.S. Environmental Protection Agency (EPA), Office of Research and Development (ORD): CMAQ (Version 5.3), Zenodo, https://doi.org/10.5281/zenodo.3379043, Washington, DC, USA, August 2019.